



**HAL**  
open science

## **Glass-forming ability and structural features of melt-quenched and gel-derived SiO<sub>2</sub>-TiO<sub>2</sub> glasses**

Alessio Zandonà, Erwan Chesneau, Gundula Hensch, Aurélien Canizarès, Joachim Deubener, Valérie Montouillout, Franck Fayon, Mathieu Allix

### ► **To cite this version:**

Alessio Zandonà, Erwan Chesneau, Gundula Hensch, Aurélien Canizarès, Joachim Deubener, et al.. Glass-forming ability and structural features of melt-quenched and gel-derived SiO<sub>2</sub>-TiO<sub>2</sub> glasses. *Journal of Non-Crystalline Solids*, 2022, 598, pp.121967. <10.1016/j.jnoncrysol.2022.121967>. <hal-03874481>

**HAL Id: hal-03874481**

**<https://hal.science/hal-03874481v1>**

Submitted on 28 Nov 2022

**HAL** is a multi-disciplinary open access archive for the deposit and dissemination of scientific research documents, whether they are published or not. The documents may come from teaching and research institutions in France or abroad, or from public or private research centers.

L'archive ouverte pluridisciplinaire **HAL**, est destinée au dépôt et à la diffusion de documents scientifiques de niveau recherche, publiés ou non, émanant des établissements d'enseignement et de recherche français ou étrangers, des laboratoires publics ou privés.



HAL Authorization

1 **Glass-forming ability and structural features of melt-quenched and gel-derived SiO<sub>2</sub>-TiO<sub>2</sub> glasses**

2  
3 Alessio Zandonà<sup>a\*</sup>, Erwan Chesneau<sup>a</sup>, Gundula Hensch<sup>b</sup>, Aurélien Canizarès<sup>a</sup>, Joachim Deubener<sup>b</sup>, Valérie  
4 Montouillout<sup>a</sup>, Franck Fayon<sup>a</sup>, Mathieu Allix<sup>a</sup>

5  
6  
7 <sup>a</sup> CNRS, CEMHTI UPR3079, Univ. Orléans, F-45071 Orléans, France

8 <sup>b</sup> Clausthal University of Technology, Institute of Non-Metallic Materials, 38678 Clausthal-Zellerfeld,  
9 Germany

10  
11 **Abstract**

12 SiO<sub>2</sub>-TiO<sub>2</sub> glasses produced by aerodynamic levitation coupled to laser heating or by sol-gel spray-drying  
13 were compared to highlight their structural differences. Glass formation was possible by melt-quenching  
14 up to 10 mol% TiO<sub>2</sub>, while higher contents led to devitrification. Raman spectroscopy and solid-state <sup>17</sup>O  
15 and <sup>29</sup>Si **magic-angle-spinning nuclear magnetic resonance** confirmed the clear emergence of Ti-O-Si  
16 bonds and a tetrahedral oxygen coordination of Ti<sup>4+</sup> leading to full network connectivity, as also  
17 substantiated by the synthesis of TiO<sub>2</sub>-doped cristobalite. In gel-derived glasses, water content induced  
18 partial network depolymerization, thereby enhancing the solubility of TiO<sub>2</sub> in the hydrous silicate matrix.  
19 However, full dehydration during heating proved challenging due to a competing tendency towards  
20 devitrification: the glass-forming range in the anhydrous binary SiO<sub>2</sub>-TiO<sub>2</sub> system does not therefore appear  
21 to be significantly enlarged by the sol-gel synthesis route.

22  
23 **Keywords:** glass-forming ability, Raman spectroscopy, solid-state NMR, titania silica glasses, cristobalite

24 \*Corresponding author: [alessio.zandona@cnrs-orleans.fr](mailto:alessio.zandona@cnrs-orleans.fr)

## 27 **1. Introduction**

28           The incorporation of  $\text{Ti}^{4+}$  in silicate melts and glasses has attracted an unceasing research interest  
29 in both geoscience and materials science.  $\text{TiO}_2$  is indeed a frequent secondary component of terrestrial and  
30 lunar rocks and has been evaluated as a sensitive indicator of magma genesis and differentiation [1–4].  
31 More recently, the precipitation of nanosized Fe-Ti-oxides during decompression has been associated to  
32 the intermittent explosive behavior of low-viscosity magmas [5]. Due to its strong tendency to segregate  
33 from the melt and crystallize, this oxide serves moreover as a widespread nucleating agent for the synthesis  
34 of glass-ceramics [6], while it represents a fundamental constituent of  $\text{SiO}_2$ - $\text{TiO}_2$  glasses/glass-ceramics  
35 that are appreciated for their low thermal expansion and catalytic activity [7–9].

36           The  $\text{Ti}^{4+}$  ion possesses an amphoteric or intermediate character with respect to those of the  
37 classically defined network formers and modifiers [10]. Its oxygen coordination in silicate melts exhibits a  
38 strong dependence on temperature, pressure and especially composition; it is generally pictured as a  
39 combination of coexisting tetrahedral, square-pyramidal and/or octahedral units [11–16]. Since low-  
40 coordinated species are predominant in silicate glasses [12,15], whereas  $\text{Ti}^{4+}$  is typically six-fold  
41 coordinated in the crystalline state [17], configurational changes are frequently associated with the  
42 precipitation of  $\text{TiO}_2$ -bearing crystals in a silicate melt [18,19]. Analogously, the glass forming ability of  
43  $\text{TiO}_2$ -containing melts has been previously evaluated in terms of the ratio between low-coordinated species  
44 and modifier-like sixfold coordinated  $\text{Ti}^{4+}$ , such as in the  $\text{SiO}_2$ - $\text{TiO}_2$  compositional system [20].

45           This latter system, extensively studied in the past due to the above-mentioned technological  
46 importance, appears as a promising candidate for elucidating the solubility and structural role of  $\text{Ti}^{4+}$  in a  
47 simplified amorphous silicate matrix. Nevertheless, literature sources spanning over at least five decades  
48 provided occasionally contrasting views on the structural features of these glasses (a short review is  
49 proposed in Section 1.1). This is partially related to their high melting temperature and strong tendency to  
50 crystallize [21–23], which make the classical melt-quench route unfavorable, leading to a preference for  
51 other synthesis methods including flame hydrolysis and sol-gel processing.

52           This work was therefore conceived as a fundamental clarification of analogies and dissimilarities  
53 between  $\text{SiO}_2$ - $\text{TiO}_2$  glasses obtained by melt-quenching (or equivalently by flame hydrolysis, involving a  
54 very high sintering temperature) and by sol-gel processing. Combining Raman spectroscopy, solid-state  
55 nuclear magnetic resonance (NMR) and molecular dynamics (MD) simulations, we succeeded in  
56 developing an all-encompassing picture of the glass-forming region and structural features of these  
57 materials.

58

### 59 **1.1 Review of relevant literature on $\text{SiO}_2$ - $\text{TiO}_2$ amorphous materials**

60 Studies based on conventional melting focused mostly on the determination of a phase diagram for  
61 the system (Fig. Sup1), involving a eutectic point at ~8 mol% TiO<sub>2</sub> and ~1550 °C [21] and a high-  
62 temperature liquid immiscibility field between ~20 mol% and ~90 mol% [23–25]. Despite the high melting  
63 temperatures and the strong devitrification tendency, some authors succeeded in characterizing SiO<sub>2</sub>-TiO<sub>2</sub>  
64 glasses synthesized by electromelting, setting the limit of glass-forming ability at 10-12 mol% TiO<sub>2</sub> [26,27]  
65 and invariably assuming a tetrahedral or mixed tetrahedral-octahedral oxygen coordination for Ti<sup>4+</sup> [26–  
66 29].

67 Nevertheless, large-scale production of monolithic glass samples has first been achieved by the  
68 flame hydrolysis method, in which a stoichiometric vapor mixture of suitable volatile precursors (such as  
69 SiCl<sub>4</sub> and TiCl<sub>4</sub>) is oxidized in a CH<sub>4</sub>-O<sub>2</sub> flame to obtain a fine glassy particulate that can be thereafter  
70 sintered at temperatures > 1700 °C [7]. The glass-forming region was macroscopically inferred to extend  
71 up to ~12.5 mol% [7]; early Raman and IR spectroscopic characterizations suggested again a tetrahedral or  
72 mixed tetrahedral-octahedral oxygen coordination of Ti<sup>4+</sup> [30–32], in agreement with the reported solubility  
73 of TiO<sub>2</sub> in cristobalite up to ~8 mol% [33]. More direct investigations performed by X-ray absorption  
74 spectroscopy (XAS) at the Ti K-edge [34,35] revealed Ti<sup>4+</sup> to be almost solely 4-fold coordinated in these  
75 glasses in the range 2-6 mol% TiO<sub>2</sub>, with an increasing amount of octahedral species (still < 30% of the  
76 total) subsequently appearing up to 11.5 mol%, where the first crystalline TiO<sub>2</sub> polymorphs were detected.  
77 At impurity levels (TiO<sub>2</sub> < 0.03 mol%), Ti<sup>4+</sup> would instead exhibit modifier-like 6-fold oxygen  
78 coordination. Later analyses by X-ray photoelectron spectroscopy [36], Raman and IR spectroscopy [37,38]  
79 and electron energy loss spectroscopy [39] did not substantially alter these views.

80 The sol-gel route, typically based on the condensation of sols containing hydrolyzed alkoxide  
81 precursors, started to be evaluated extensively in the 1980s as a possible alternative to the high melting  
82 temperatures of SiO<sub>2</sub>-TiO<sub>2</sub> mixtures [40–42]; the potential use of these materials as porous substrates for  
83 catalytic applications particularly boosted scientific investigations [8]. Nevertheless, the choice of suitable  
84 synthesis parameters resulted crucial to avoid phase separation already in the sols or in the gels [43–  
85 45,45,46]. The need for drying the gels at relatively high temperatures to obtain fully interconnected glasses,  
86 moreover, appeared in clear conflict with the low thermal stability of these glasses [41,47,48]; notice that  
87 water could be still detected in SiO<sub>2</sub>-TiO<sub>2</sub> amorphous materials after annealing at 900 °C [40] and a similar  
88 H<sub>2</sub>O persistence was reported in gel-derived SiO<sub>2</sub> glass [49–52].

89 All these factors made the structural investigation of gel-derived SiO<sub>2</sub>-TiO<sub>2</sub> glasses rather  
90 challenging. For instance, above ~6 mol% TiO<sub>2</sub>, heterogeneity and TiO<sub>2</sub> crystallization affected the samples  
91 employed by Henderson and coworkers for their Raman and XAS studies [15,41,53–55]. Despite this, they  
92 inferred a mixed 4-fold and 5-fold coordination for Ti<sup>4+</sup> in the glass, possibly involving the formation of  
93 oxygen triclusters; they associated 6-fold coordinated species to Ti-rich clusters. Concurrently, other

94 authors [56–63] adopted a multipronged approach including solid-state NMR, X-ray and neutron diffraction  
95 and XAS to elucidate the structural evolution of SiO<sub>2</sub>-TiO<sub>2</sub> gels during condensation and annealing.  
96 According to their ultimate results, four possible environments are suggested for Ti<sup>4+</sup> in these materials: 1)  
97 distorted octahedral oxygen coordination, prevalently in gels treated below 250 °C and possibly  
98 corresponding to a tetrahedron with two further bonds to hydroxyl groups; more regular 2) tetrahedral and  
99 3) octahedral units, dispersed in the amorphous structure of gel-derived glasses treated at relatively high  
100 temperature; 4) six-fold oxygen coordination in phase-separated TiO<sub>2</sub>-rich clusters and crystals.

101

## 102 **2. Experimental**

### 103 *2.1. Sol-gel glasses*

104 Sol-gel glasses were produced as spray-dried nanobeads according to the method presented in a  
105 previous publication [9]. Two solutions were prepared, homogenized separately and mixed together in the  
106 desired ratios shortly before being spray-dried. The first solution contained tetraethoxysilane (TEOS, 99.0%  
107 (GC), Fluka), isopropanol, deionized water as a hydrolysis agent (molar ratio TEOS/H<sub>2</sub>O = 0.25) and  
108 concentrated nitric acid (69%, Fluka) to adjust the pH to 1. The second solution was obtained by mixing  
109 equimolar amounts of Ti-butoxide (97.0%, Sigma-Aldrich) and ethyl acetoacetate (99.0%, Sigma-Aldrich)  
110 in isopropanol. Mixed solutions corresponding to samples with 5, 8, 10 and 17 mol% TiO<sub>2</sub> (respectively  
111 T5s, T8s, T10s and T17s in the following) were nebulized into a tube furnace set at 200 °C using an aerosol  
112 atomizer (Atomizer, AGK 2000, Palas) operated with pressurized air (2.8 bar); the resulting nanobeads  
113 (diameter between 50 and 200 nm) were collected from a particle filter at the other end of the furnace.  
114 Higher TiO<sub>2</sub> loadings (e.g. from 25 to 50 mol%) could be sprayed but proved unstable to the subsequent  
115 treatment at 600 °C (SI section, Fig. Sup2); they were therefore discarded from our further analyses. For  
116 the production of a glass containing 8 mol% TiO<sub>2</sub> and enriched in <sup>17</sup>O, the same procedure was applied,  
117 using <sup>17</sup>O-enriched water (enrichment degree: 40%, Cortecnet) for the hydrolysis of TEOS; the sample is  
118 noted as T8s(<sup>17</sup>O).

119

### 120 *2.2. Melt-quenched glasses*

121 Melt-quenched glasses were prepared by aerodynamic levitation coupled to CO<sub>2</sub> laser heating  
122 (ADL), using a setup described in a previous work [64]. SiO<sub>2</sub> (Chempur, 99.9%) and TiO<sub>2</sub> (Evonik,  
123 Aeroxide TiO<sub>2</sub> P 25, 99.5%) powders were mixed thoroughly in an agate mortar and pressed into pellets of  
124 approximately 1 g. Small chunks of the pellets weighing from 10 to 50 mg were then melted using O<sub>2</sub> as a  
125 levitation gas, gradually increasing the laser power until reaching 1900-2100 °C (as recorded by two  
126 pyrometers). The levitated droplet was left at this temperature for a few seconds and then quenched by  
127 cutting the laser power; the cooling rate is estimated to be in the order of 300 K s<sup>-1</sup> or more [64]. Using this

128 method, several glassy beads containing 0, 0.5, 1, 2, 4, 6, 8 and 10 mol% could be prepared; they were  
129 accordingly named T0m, T0.5m, T1m, T2m, T4m, T6m, T8m, T10m (-m for melt-quenched). In the range  
130 T0m-T6m, macroscopically homogeneous colorless beads could reproducibly be obtained, whereas TiO<sub>2</sub>-  
131 richer compositions frequently exhibited opaque regions due to the crystallization of anatase, as confirmed  
132 by Raman spectroscopy. It was impossible to reliably obtain glassy samples with TiO<sub>2</sub> contents >10 mol%.  
133 All glassy beads were very rich in bubbles, due to the high viscosity of the materials at the employed melting  
134 temperatures, which also resulted in occasionally poor chemical homogenization of the melts (confirmed  
135 by SEM). Nevertheless, lower viscosities could not be attained due to physical limitations, since Si and Ti  
136 are increasingly volatile above 2000 °C [65]. An analytical strategy based on the analysis of a large number  
137 of samples was therefore adopted to overcome the uncertainties possibly arising from the occasional  
138 heterogeneity of the samples (see below).

139 In the attempt of synthesizing a melt-quenched glass enriched in <sup>17</sup>O, the as-sprayed sol-gel sample  
140 T8s(<sup>17</sup>O) was placed in a tungsten crucible and melted at 1800 °C for 1 h in vacuum (to avoid exchanges  
141 with the atmospheric <sup>16</sup>O<sub>2</sub>), using a Setaram DTA/TGA SETSYS Evo 2400. The so-obtained material was  
142 partially crystallized; it is referred in the following as T8m(<sup>17</sup>O).

143

### 144 2.3. Heat treatments

145 The as-prepared sol-gel materials required a further annealing stage to fully decompose the residues  
146 of their organic precursors, as also observed before [9]. A treatment at 450 °C for 12 h in air resulted  
147 insufficient: a strong photoluminescence still prevented the acquisition of Raman spectra with the selected  
148 laser line at 514 nm; heating at 600 °C for 12 h was found more suitable, although the glasses still contained  
149 substantial amounts of water. To dehydrate them, several drying protocols were then attempted in air using  
150 conventional laboratory furnaces, as detailed in Fig. 3-b: heating ramps were kept at 5 K s<sup>-1</sup>, testing  
151 maximum temperatures between 900 °C and 1200 °C and isothermal segments from 1 h to 30 h.

152 In the case of sample T8s(<sup>17</sup>O), the pre-emptive heat treatment at 600 °C was performed in Ar  
153 using a Setaram DTA/TGA SETSYS Evo 2400, to avoid exchanges with <sup>16</sup>O<sub>2</sub> from the atmosphere;  
154 however, the sample still exhibited photoluminescence, so that the as-sprayed powder was subsequently  
155 treated also at 800 °C for 12 h, to enable its characterization by Raman spectroscopy. Different  
156 decomposition kinetics of the organic precursors according to the employed atmosphere have been  
157 previously reported [40].

158 TiO<sub>2</sub>-bearing cristobalite was synthesized according to the procedure described by previous authors  
159 [33]: sample T5s was placed in a hot furnace at 1450 °C for 2 h and then quenched in air. For comparison,  
160 a TiO<sub>2</sub>-free cristobalite sample was similarly produced, treating our SiO<sub>2</sub> raw material at 1600 °C for 4 h.  
161 These samples are respectively named as T5crist and T0crist in the following treatment.

162  
163  
164  
165  
166  
167  
168  
169  
170  
171  
172  
173  
174  
175  
176  
177  
178  
179  
180  
181  
182  
183  
184  
185  
186  
187  
188  
189  
190  
191  
192  
193

#### 2.4. Raman spectroscopy

Raman spectra were collected in parallel polarization using a Renishaw InVia Qontor spectrometer, mounting an Ar green laser (514 nm) and a holographic grating of 1800 lines/mm. The nominal laser power was generally set at 50 mW, but samples containing high amounts of TiO<sub>2</sub> and/or crystalline TiO<sub>2</sub> polymorphs required attenuation down to 1% of this power to avoid detector saturation. The measurements were performed with 15 s integration time and 6 accumulations, focusing 30-40 μm below the surface of the melt-quenched beads or on the gel-derived nanosized powders with a 50x objective. Numerous melt-quenched beads of each nominal composition were analyzed at several locations, to avoid partially crystallized regions and average out possible compositional inaccuracies deriving from occasionally poor homogenization of the melts. In the following data treatment (Fig. 2), at least three spectra for each melt-quenched composition were analyzed, after a first selection among several candidates.

Data evaluation involved a simple baseline subtraction between 80 and 1300 cm<sup>-1</sup> (Figs. 3 and 4 examine a much wider spectral range and therefore report the raw spectra); the spectra were then normalized to their maximum intensity. To verify the appearance and growth of a Raman band at ~685 cm<sup>-1</sup> (marked as *T<sub>I</sub>* in the following), the spectra shown in Figure 1 were smoothed and differentiated in the range 620-770 cm<sup>-1</sup>; the slope of the first derivative was used to mathematically infer the concavity variation in this spectral region. Interpretation of the Raman spectra of crystalline materials was facilitated by the online consultation of the RRUFF database [66]: reference IDs are accordingly reported in the text.

#### 2.5. X-ray diffraction (XRD)

The samples were characterized by XRD using a D8 Advance Bruker laboratory diffractometer (Bragg-Brentano geometry, Cu Kα<sub>1,2</sub> incident radiation, LynxEye XE line detector). The powders were placed on low-background flat Si sample holders and dispersed with a few ethanol droplets. Lattice parameters were computed by Le-Bail fits using the software HighScore Plus (Panalytical).

#### 2.6. Transmission electron microscopy (TEM)

Sample T8m(<sup>17</sup>O) was examined in a Philips CM20 TEM operated at 200 kV, performing bright- and dark-field imaging, selected area electron diffraction (SAED) and energy-dispersive X-ray spectroscopy (EDX) measurements. The powder was dispersed in ethanol, after which a droplet was deposited and dried on a copper grid layered by an amorphous holey carbon film.

194 *2.7. Molecular dynamics simulation and DFT GIPAW computation*

195 Classical molecular dynamics (MD) model structures of T10m glass were generated with rigid ion  
196 potentials using the DL\_POLY 4 package, whose details are reported elsewhere [67,68]. This composition  
197 has been chosen to remain close to that of melt-quenched glasses while increasing the number of statistically  
198 relevant titanium atoms in the cell. Cubic boxes with 150 atoms were used and the edge lengths were  
199 adjusted to match the experimental density [7]. We used a previously proposed force field [69] in which  
200 interactions between Si-O, Ti-O and O-O are formalized by a Morse potential. Initial random structures  
201 were first equilibrated by a 100 ps NVT run at high temperature (3500 K), followed by quenching at a rate  
202 of 2.5 K ps<sup>-1</sup> from 3500 K to 300 K. Six structures were created to increase the statistics.

203 For all obtained structural models, the atomic positions were optimized by DFT using the CASTEP  
204 package [70]. Computations of NMR chemical shielding and electric field gradient tensors were then  
205 performed using the Gauge Including Projector Augmented Waves (GIPAW) [71] and the Projector  
206 Augmented Waves (PAW) [72] methods respectively, as implemented in CASTEP. All computations were  
207 performed using the GGA PBE functional [73] and ultrasoft pseudopotentials (Materials Studio 7.0)  
208 generated “on-the-fly” [74]. Isotropic chemical shifts were calibrated based on series of computations  
209 performed on model crystalline systems of known structures, according to the relationships [75]:

210 
$$\delta(^{29}\text{Si}) = -0.921 \sigma(^{29}\text{Si}) + 289$$

211 
$$\delta(^{17}\text{O}) = -0.946 \sigma(^{17}\text{O}) + 252$$

212 where  $\delta$  is the isotropic chemical shift and  $\sigma$  the corresponding chemical shielding.

213 NMR parameters were also computed for anatase and rutile TiO<sub>2</sub> models considering supercells of  
214 384 and 576 atoms, respectively, and using the same setting as for MD structures. Structural and GIPAW  
215 calculations were analysed using a homemade python code. Atoms were clustered as a function of their  
216 speciation (i.e. coordination numbers, atom-linked...), calculating property distributions for each  
217 speciation. Distributions were smoothed by applying a Gaussian broadening to each point with broadness  
218 equal to the standard deviation of the dataset. The cut-off radius used to perform structural analyses was set  
219 to 2.2 Å for Si-O and Ti-O, corresponding to the first minimum of the partial distribution function. All  
220 structural analyses reported in the text below were performed on these DFT-optimized structures.

221

222 *2.8. Solid-state nuclear magnetic resonance (NMR)*

223 Only reproducibly amorphous samples were characterized by solid-state NMR, crushing and  
224 grinding several beads; the resulting powder was filled into ZrO<sub>2</sub> rotors. In addition, partially crystallized  
225 T8m(<sup>17</sup>O) was also measured, to support the interpretation of <sup>17</sup>O Magic Angle Spinning (MAS) NMR  
226 spectra. <sup>29</sup>Si MAS NMR spectra were acquired on a Bruker Avance III spectrometer operating at a magnetic  
227 field of 7.0 T (<sup>29</sup>Si Larmor frequency of  $\nu_0=59.6$  MHz) using a 4 mm probe. Spectra were recorded at a

228 spinning rate of 10 kHz using a 30° flip angle (radio frequency field of 55 kHz) and a recycle delay of 60 s  
229 to insure complete relaxation of the magnetization. Between 1000 and 3000 transients were collected for  
230 each spectrum. <sup>29</sup>Si chemical shifts are referenced relative to tetramethylsilane (TMS) at 0 ppm. Because  
231 the T8m(<sup>17</sup>O) sample was only available in limited amount, a Carr-Purcell-Meiboom-Gill (CPMG) echo-  
232 train acquisition [76,77] was used to enhance the signal-to-noise ratio by summing 256 echoes equally  
233 spaced by a duration of 5.2 ms.

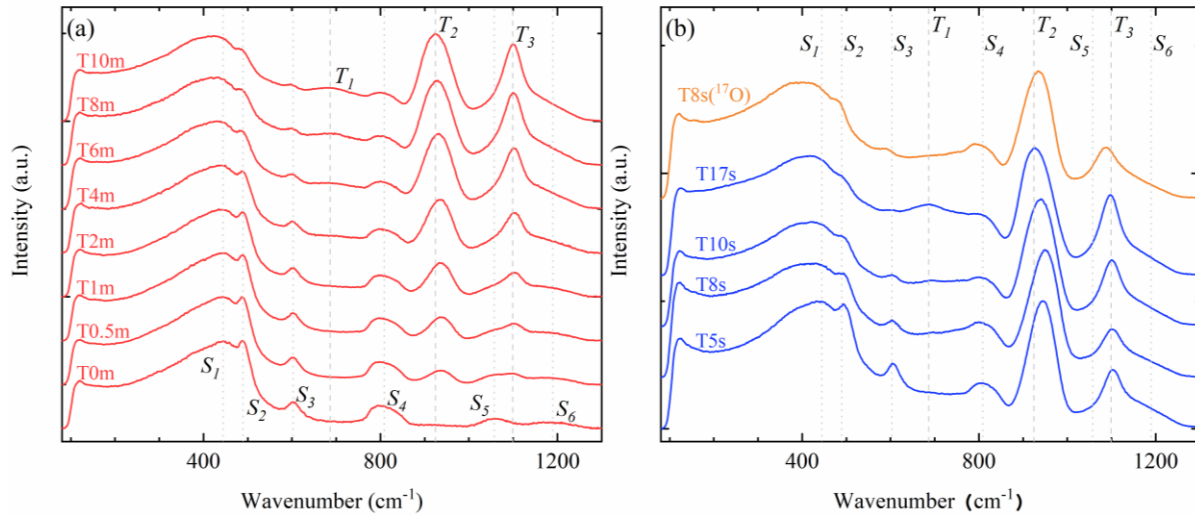
234 <sup>17</sup>O MAS NMR spectra were acquired on a Bruker Avance III spectrometer operating at a magnetic  
235 field of 17.6 T (<sup>17</sup>O Larmor frequency of  $\nu_0=101.7$  MHz) using a 2.5 mm probe. Quantitative spectra were  
236 recorded at a spinning rate of 33.33 kHz using a small flip angle of 10° (corresponding to a pulse duration  
237 of 0.55  $\mu$ s). Between 16384 and 20480 transients were co-added with a recycle delay of 0.5 s. <sup>17</sup>O chemical  
238 shifts are referenced relative to water at 0 ppm. <sup>17</sup>O-<sup>1</sup>H polarization transfer experiments allowing the  
239 selective observation of T-O-H moieties were performed using a refocused-INEPT [78,79] sequence with  
240 a SR421 recoupling block [80,81]. The RF field strengths for the  $\pi/2$  and  $\pi$  pulses on the <sup>17</sup>O and <sup>1</sup>H channels  
241 were set to 20 and 78 kHz, respectively, while a <sup>1</sup>H RF field strength of 66.66 kHz corresponding to the  
242  $2\omega_R$  condition was used for the recoupling block. Recoupling delay was kept short (120  $\mu$ s) in order to  
243 selectively probe short-range O-H distances.

244 <sup>29</sup>Si FID were processed through a homemade python code using nmrglue and numpy libraries  
245 [82,83]. Gaussian apodization centered at the top of the signal was applied prior to Fourier transform with  
246 line broadening of 25 Hz for <sup>29</sup>Si and <sup>17</sup>O. Simulations of <sup>17</sup>O spectra were done with Dmfit software [84]  
247 and <sup>29</sup>Si ones were done using fNMR package [85].

248

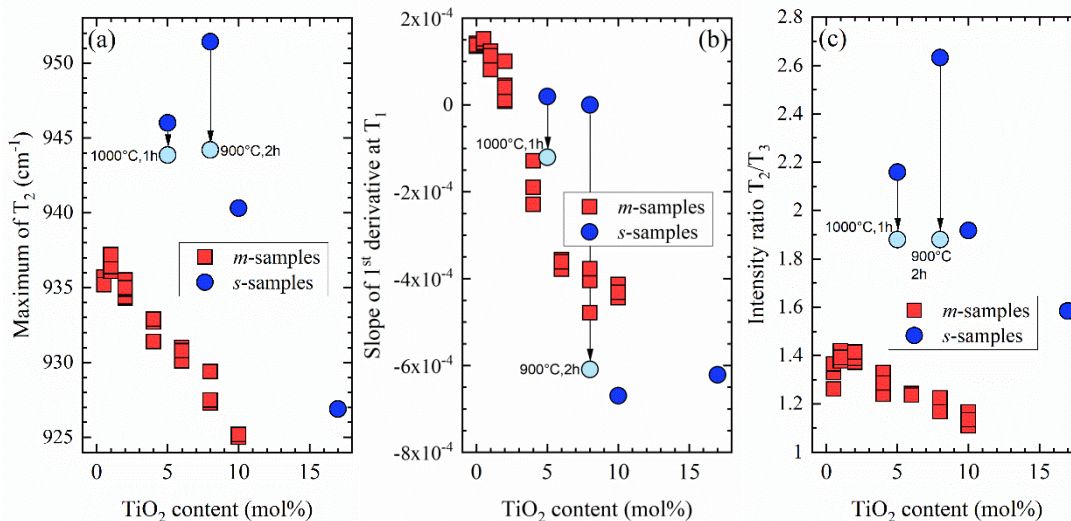
### 249 **3. Results**

#### 250 *3.1 Glass-forming ability and overall examination*



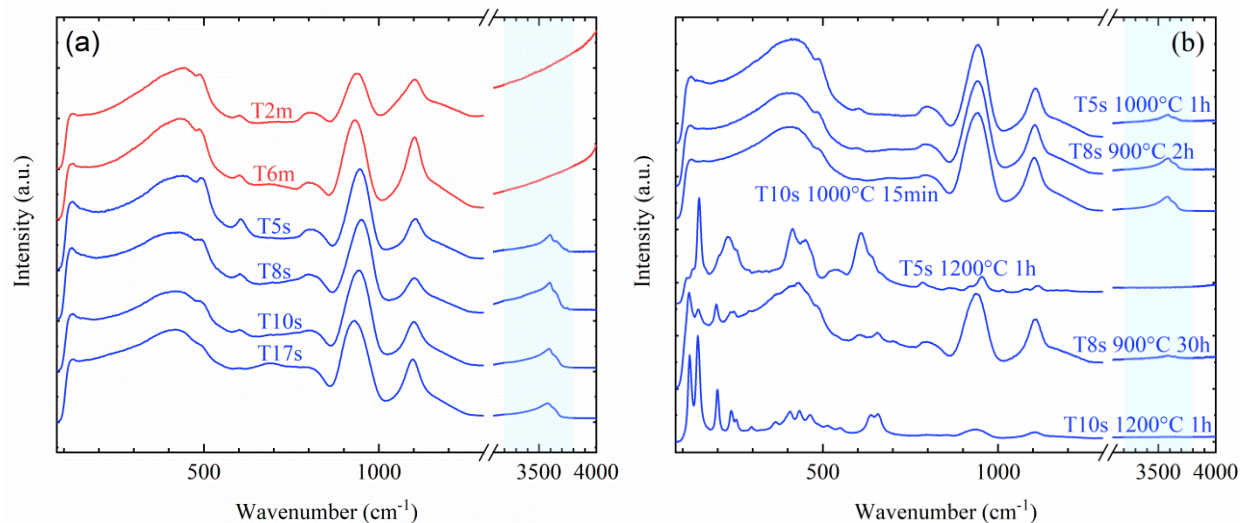
251  
 252 Figure 1. Raman spectra acquired from SiO<sub>2</sub>-TiO<sub>2</sub> glasses obtained by different synthesis methods. a) Melt-  
 253 quenched samples; b) gel-derived materials, treated at 600 °C for 12 h in air, excluding T8s(<sup>17</sup>O) which was  
 254 treated in Ar at 800 °C for 12 h. The main characteristic bands for vitreous SiO<sub>2</sub> are labelled as S<sub>1</sub>, S<sub>2</sub>, S<sub>3</sub>,  
 255 S<sub>4</sub>, S<sub>5</sub> and S<sub>6</sub>, while those related to the incorporation of Ti<sup>4+</sup> are identified by T<sub>1</sub>, T<sub>2</sub> and T<sub>3</sub>; vertical lines  
 256 are kept at the same position in both figures to facilitate the comparison.

257  
 258 The Raman spectra collected from melt-quenched materials (Fig 1-a) confirmed the formation of  
 259 glasses and the successful incorporation of Ti<sup>4+</sup> up to 10 mol% TiO<sub>2</sub>. Sample T0m exhibited the typical  
 260 vibrational features of vitreous SiO<sub>2</sub>, labelled from S<sub>1</sub> to S<sub>6</sub>. According to the available literature, S<sub>1</sub> and S<sub>4</sub>  
 261 (the latter one possibly involving a LO-TO splitting) can be assigned to the vibrations of Si-O-Si linkages  
 262 in the glass network [86–88]; S<sub>2</sub> and S<sub>3</sub> are also known as “defect lines”, respectively stemming from the  
 263 breathing modes of four- and three-membered rings of SiO<sub>4</sub> tetrahedra [89,90]; S<sub>5</sub> and S<sub>6</sub> were previously  
 264 related to the asymmetric stretching of bridging oxygens linking SiO<sub>4</sub> tetrahedra, again with a LO-TO  
 265 splitting [86–88] or possibly corresponding to two different sets of stretching vibrations [91]. Upon TiO<sub>2</sub>  
 266 incorporation, the broad maximum S<sub>1</sub> shifted to lower wavenumbers, while S<sub>2</sub> and S<sub>3</sub> gradually subsided.  
 267 In parallel, three supplementary Raman features became visible and increased in intensity, labelled as T<sub>1</sub>,  
 268 T<sub>2</sub> and T<sub>3</sub>. The assignment of these bands is controversial in the available literature and will be addressed  
 269 in higher detail in the Discussion section. Nevertheless, the position of the maximum of T<sub>2</sub> (Fig. 2-a), the  
 270 concavity of the Raman spectra at T<sub>1</sub> (i.e. the slope of their 1<sup>st</sup> derivative, Fig. 2-b) and the intensity ratio  
 271 T<sub>2</sub>/T<sub>3</sub> (Fig. 2-c) exhibited an approximately linear correlation with the TiO<sub>2</sub> content of the melt-quenched  
 272 glasses.



273  
 274 Figure 2. Representative indices computed from the Raman spectra of melt-quenched and gel-derived  
 275 glasses ( $T_8s(^{17}\text{O})$  was disregarded due to the isotopic shift). a) Location of the maximum intensity for the  
 276 Raman band labeled as  $T_2$ ; b) slope of the 1<sup>st</sup> derivative of the Raman signal at the position of  $T_1$ ; c) intensity  
 277 ratio between  $T_2$  and  $T_3$ . Light blue circles represent the values obtained for partially dehydrated (and still  
 278 amorphous) gel-derived samples, namely T5s treated at 1000 °C for 1 h and T8s treated at 900 °C for 2 h  
 279 (the spectra are reported in Fig. 3).

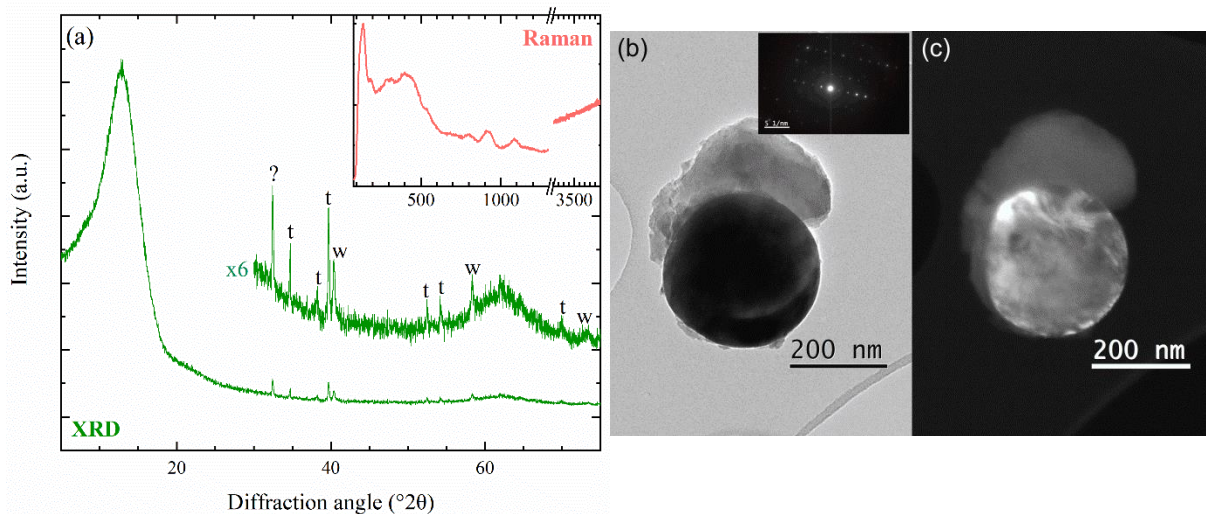
280  
 281 Gel-derived glasses treated at 600 °C for 12 hours in air (Fig 1-b) exhibited strong similarities with  
 282 those of their melt-quenched counterparts; amorphous materials could be easily obtained up to 17 mol%  
 283 TiO<sub>2</sub>. However, the computation of the above-introduced indices (Fig. 2) highlighted a general shift of  $T_2$   
 284 to higher wavenumbers, a lower visibility of  $T_1$  and a much lower intensity of  $T_3$  in comparison to melt-  
 285 quenched glasses of similar composition; the defect bands  $S_2$  and  $S_3$  appeared moreover more pronounced  
 286 (compare for instance T5s and T6m). As for sample  $T_8s(^{17}\text{O})$  (dried at 800 °C for 12 in Ar), its spectrum  
 287 matched well with that of T8s but exhibited a slight overall shift to lower wavenumbers, in line with  
 288 previous observations of the Raman spectrum of  $^{18}\text{O}$ -substituted SiO<sub>2</sub> [87]. The noticed differences between  
 289 melt-quenched and gel-derived glasses were ascribed to the non-negligible water content of these latter, as  
 290 demonstrated by Raman spectra collected over a wider range (Fig. 3). A broad band assignable to OH  
 291 stretching vibrations was indeed clearly identifiable at  $\sim 3600 \text{ cm}^{-1}$  [92,93], while it was absent in melt-  
 292 quenched materials.



293  
 294 Figure 3. Raman spectra collected over a wider range (80 – 4200  $\text{cm}^{-1}$ ) from some of the samples. a) Melt-  
 295 quenched glasses (as-prepared) and gel-derived glasses (pre-treated at 600 °C for 12 h), manifesting the  
 296 presence of water in their structure; b) gel-derived glasses treated at various temperatures for up to 30 h,  
 297 invariably exhibiting the onset of crystallization before full dehydration was completed.

298  
 299 Samples T5s, T8s and T10s were subjected to several tentative heat treatments at temperatures  
 300 between 900 °C and 1200 °C: interestingly, partial dehydration of T5s (at 1000 °C for 1 h) and of T8s (at  
 301 900 °C for 2 h) led their spectra to resemble more closely those of their melt-quenched analogs, with a  
 302 visible broadening of the defect bands  $S_2$  and  $S_3$  and an increase in the relative intensity of  $T_3$ , mirrored by  
 303 a variation in the indices plotted on Fig. 2. However, full dehydration proved challenging to achieve before  
 304 the onset of crystallization, marked by the appearance of sharper bands assignable to  $\text{TiO}_2(\text{B})$ , anatase [94],  
 305 rutile and cristobalite (see references: [RRUFF-ID: R050031] and [RRUFF-ID: X050046]). As for T17s,  
 306 previous investigations evidenced the emergence of  $\text{TiO}_2(\text{B})$  and anatase crystals even only after 15 min at  
 307 800 °C [9]. Since treatments below the melting point were invariably affected by partial crystallization, full  
 308 dehydration of gel-derived T8s( $^{17}\text{O}$ ) was attempted by complete melting at 1800 °C and subsequent  
 309 quenching in vacuum (to avoid loss of  $^{17}\text{O}$  to the atmosphere). The characterization by XRD and TEM of  
 310 the resulting T8m( $^{17}\text{O}$ ) revealed that it was still for the most part amorphous (Fig. 4); however, the  
 311 crystallization of few highly Ti-enriched noduli (composition qualitatively confirmed by EDX) could be  
 312 detected, whose diffraction pattern was indexable as an oxygen-interstitial solid solution derived from  
 313 metallic Ti [95], such as  $\text{Ti}_6\text{O}$  [ICDD 01-072-1471] or  $\text{Ti}_3\text{O}$  [ICDD 01-072-1806]. The Raman spectrum  
 314 revealed the appearance at low wavenumbers of intense vibrational features characteristic for Ti-bearing  
 315 crystals, which however did not completely obliterate the spectrum of the glass, hinting at a very low

316 crystalline volume fraction. Judging from its Raman spectrum, the residual glass was anhydrous and still  
 317 contained some  $\text{TiO}_2$  despite the partial crystallization, as confirmed by the clear persistence of the bands  
 318 labeled as  $T_2$  and  $T_3$  and the absence of vibrational features at  $\sim 3600\text{ cm}^{-1}$ .  
 319



320  
 321 Figure 4. Experimental characterization of sample T8m( $^{17}\text{O}$ ), obtained by melting gel-derived T8s( $^{17}\text{O}$ ) at  
 322  $1800\text{ }^\circ\text{C}$  in vacuum. a) XRD pattern and Raman spectrum (inset) of the sample, manifesting the formation  
 323 of small amounts of Ti-suboxide solid solutions (indexable as  $\text{Ti}_6\text{O}$  or  $\text{Ti}_3\text{O}$ ) in an otherwise fully anhydrous  
 324 and amorphous matrix (labels:  $t$  for Ti-suboxide solid solution,  $w$  for rests of the tungsten crucible). b)  
 325 Bright-field and c) dark-field TEM micrographs of one of the Ti-enriched crystalline noduli found in the  
 326 sample, with an inset exemplifying the well-defined electron diffraction patterns obtainable from them.

327  
 328 **3.2 Structural characterization**

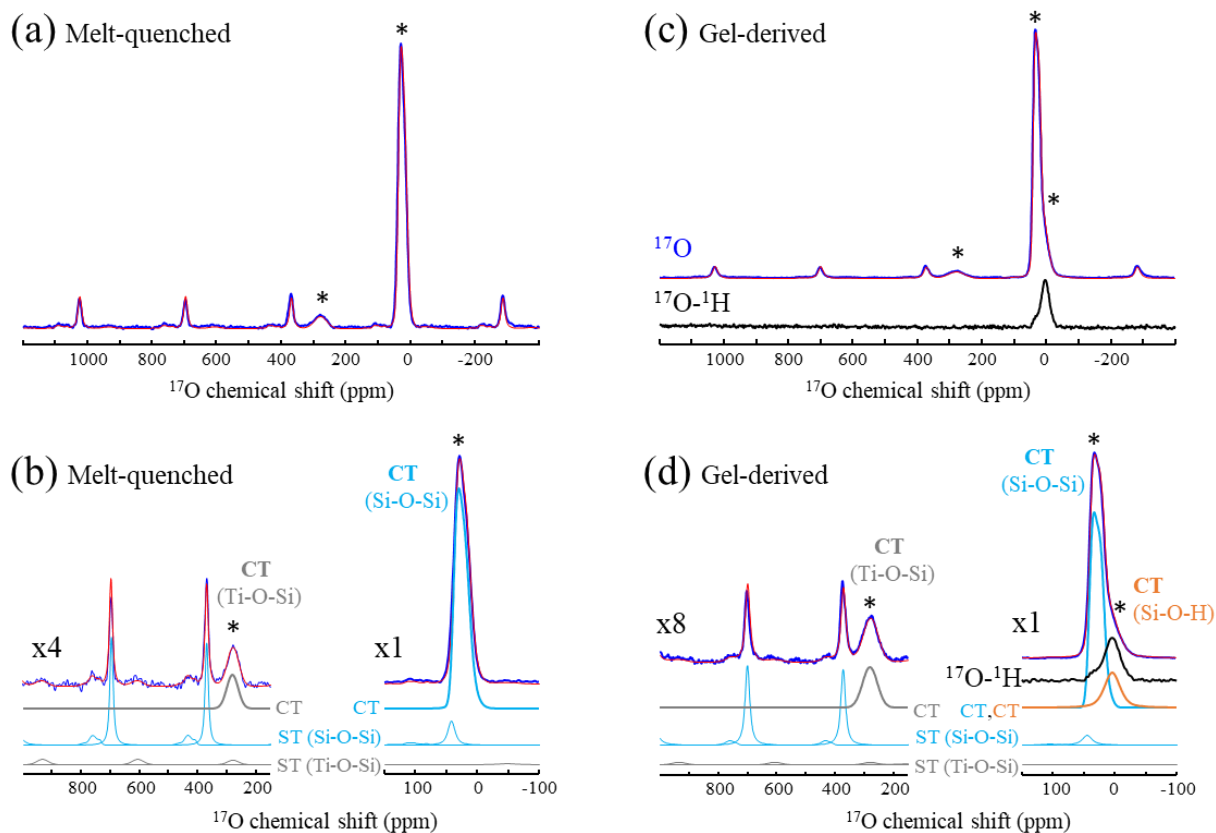
329 **3.2.1 Melt-quenched samples**

330 Further investigations of the incorporation of  $\text{Ti}^{4+}$  in silica glasses were conducted using  $^{17}\text{O}$  and  
 331  $^{29}\text{Si}$  solid-state NMR, which have been shown to provide detailed information about chemical bonding and  
 332 local structures in a variety of glasses [96–101]. For this purpose, a melt-quenched  $^{17}\text{O}$ -enriched glass with  
 333 nominal 8 mol%  $\text{TiO}_2$  was synthesized as described above (Section 2.2).

334 As shown in Figure 5, the quantitative  $^{17}\text{O}$  MAS NMR spectrum of sample T8m( $^{17}\text{O}$ ) exhibits two  
 335 well-resolved  $^{17}\text{O}$  central transition (CT) resonances and their associated satellite-transition (ST) spinning  
 336 sideband manifolds, thereby revealing two distinct oxygen bonding environments in the glass structure.  
 337 According to  $^{17}\text{O}$  NMR literature data on  $\text{SiO}_2\text{-TiO}_2$  materials [45,57,62], the intense line centered at 24.7  
 338 ppm and the broader one at 280 ppm can be assigned to bridging  $\text{O}_{2\text{Si}}$  and  $\text{O}_{1\text{Ti-1Si}}$  environments,

339 respectively. For the O\_2Si moieties, the  $^{17}\text{O}$  average isotropic chemical shift and quadrupolar coupling  
340 values ( $\delta_{\text{iso}} = 41.3$  ppm,  $C_Q = 5.33$  MHz) obtained from the CT lineshape simulation assuming Gaussian  
341 distributions of  $\delta_{\text{iso}}$  and  $C_Q$  are close to those reported for pure silica glass [102,103] (Tab. Sup1). Getting  
342  $\delta_{\text{iso}}$  and  $C_Q$  values for the O-1Ti-1Si resonance is more difficult because it shows a featureless central  
343 transition, in addition to satellite transition sidebands of low intensities. We only report the position of the  
344 CT barycenter ( $\delta_{1/2}$ ) and notice that the  $\langle \pm 3/2, \pm 1/2 \rangle$  satellite transition sidebands are much broader than  
345 those of the O-2Si resonance suggesting a larger distribution of  $^{17}\text{O}$  isotropic chemical shift for the O-1Ti-  
346 1Si moieties. Except for the ST spinning sidebands of O\_2Si and O\_1Ti-1Si, we note the absence of signals  
347 in the 400-800 ppm chemical shift range associated to oxygen atoms bonded to four, three or two titanium  
348 atoms [104]. The relative proportions of O\_2Si and O\_1Ti-1Si environments obtained from the fit of the  
349 spectrum (tacking into account all ST contributions) are 93% and 7%, respectively. This amount of Si-O-  
350 Ti bridging bonds is lower than expected (15 %) from the nominal composition, assuming a homogenous  
351  $^{17}\text{O}$ -enrichment of all T-O-T linkages in a fully polymerized random network of  $\text{SiO}_4$  and  $\text{TiO}_4$  tetrahedra.  
352 Since XRD and TEM revealed the formation of pseudo-metallic Ti-rich noduli in the sample, the observed  
353 lower proportion of O\_1Ti-1Si contributions is likely due to a deviation from the starting composition of  
354 the glass, i.e. to a lower final  $\text{TiO}_2$  content than the nominal. Nevertheless, this does not affect the overall  
355 interpretation of the  $^{17}\text{O}$  MAS spectra.

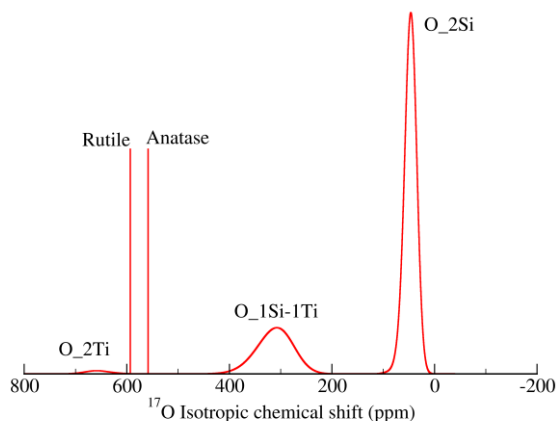
356



357  
 358 Figure 5.  $^{17}\text{O}$  MAS NMR spectra of  $^{17}\text{O}$ -enriched glasses: (a,b) melt-quenched T8m( $^{17}\text{O}$ ) and (c,d) gel-  
 359 derived T8s( $^{17}\text{O}$ ), recorded at 17.6 T with a spinning rate of 33 kHz. The  $^{17}\text{O}$ - $^1\text{H}$  MAS spectrum of T8s( $^{17}\text{O}$ )  
 360 recorded using refocused-INEPT [78,79] polarization transfer with SR4<sub>2</sub><sup>1</sup> dipolar recoupling [80] is shown  
 361 in black in (c,d). Expansions of the -100 to 150 and 150 to 1000 ppm frequency ranges are shown in (b,d).  
 362 Experimental spectra and their simulations correspond to dark blue and red lines, respectively. CT lines and  
 363 ST spinning sidebands patterns of O<sub>2</sub>Si, O<sub>1</sub>Si-1Ti and O<sub>1</sub>Si-1H contributions are shown as light blue,  
 364 grey and black lines, respectively.

365  
 366 To support the interpretation of the  $^{17}\text{O}$  NMR results, DFT GIPAW computations of  $^{17}\text{O}$  chemical  
 367 shifts were performed for structural models with composition T10m. Six amorphous structures of 150 atoms  
 368 were generated by classical force field molecular dynamics (MD) simulations and relaxed by DFT (at 0 K).  
 369 Structural details of these models are given in Table Sup2 (see also .cif files and Fig. Sup4 in the  
 370 supplementary materials). In all cases, MD simulations led to a fully polymerized tetrahedral network  
 371 containing only SiO<sub>4</sub> and TiO<sub>4</sub> units, with no other higher-coordination polyhedral species (e.g. 5-fold or  
 372 6-fold coordinated Ti<sup>4+</sup>, 5-fold coordinated Si<sup>4+</sup>). The proportion of Si-O-Ti and Ti-O-Ti linkages exhibits  
 373 a slight variability but, on average over the six structures, corresponds respectively to 18 and 1 % of the  
 374 oxygen content, as expected from composition and assuming a random distribution of TiO<sub>4</sub> units in the

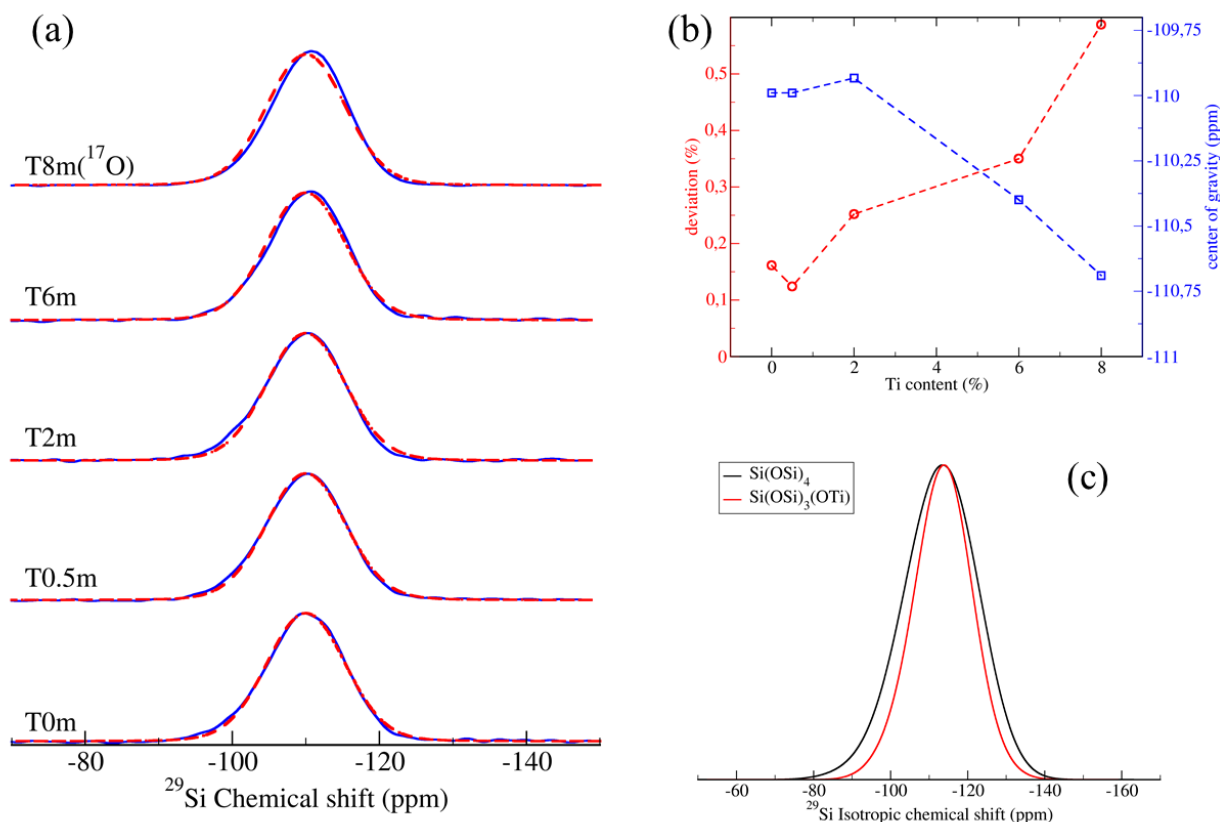
375 network. The average Ti-O bond length (1.83 Å) is found to be larger than the Si-O one (1.63 Å), in  
 376 agreement with their ionic radii [105]; similarly, the average Si-O-Si bond angle (147.9°) is smaller than  
 377 the Si-O-Ti one (150.1°). For the six amorphous structures, DFT GIPAW calculations lead to average <sup>17</sup>O  
 378 isotropic chemical shift values of about 47 ppm for O\_2Si and 312 ppm for O\_1Si-1Ti environments  
 379 (Figure 6, Table Sup3), in agreement with the proposed assignment. Moreover, the computations predict  
 380 an average <sup>17</sup>O chemical shift difference of 265 ppm between oxygen atoms bridging two SiO<sub>4</sub> and those  
 381 bridging one SiO<sub>4</sub> and one TiO<sub>4</sub> tetrahedral unit, with a larger distribution of <sup>17</sup>O isotropic chemical shift  
 382 for the latter. These results closely mimic the observed frequency difference between the two <sup>17</sup>O signals  
 383 (255.3 ppm), as well as the observed larger broadening of the O\_1Si-1Ti <+3/2,+1/2> satellite transition  
 384 sidebands, strongly supporting the formation of a fully polymerized silica-like network incorporating TiO<sub>4</sub>  
 385 tetrahedral units up to several mol% TiO<sub>2</sub>.  
 386



387  
 388 Figure 6. <sup>17</sup>O isotropic chemical shift distributions obtained from GIPAW calculations for the MD structural  
 389 models with 10 mol% TiO<sub>2</sub>. Average isotropic chemical shifts (and standard deviations) are 47.1 (8.7),  
 390 312.1 (25.1) and 656.1 (17.1) ppm for O\_2Si, O\_1Si\_1Ti and O\_2Ti environments in the MD models.  
 391 Results of GIPAW calculations for O\_3Ti environments in anatase and rutile TiO<sub>2</sub> are also provided for  
 392 comparison.

393 The local structure of melt-quenched glasses up to 8 mol% TiO<sub>2</sub> was also investigated using <sup>29</sup>Si  
 394 solid-state NMR. As depicted in Figure 7-a, the <sup>29</sup>Si MAS spectra of melt-quenched samples were very  
 395 similar, almost independently of the titanium content. For the TiO<sub>2</sub>-free silica glass, the <sup>29</sup>Si spectrum  
 396 showed a broad resonance at -110.0 ppm characteristic for Q<sup>4</sup> units and only a slight shift of 0.7 ppm  
 397 toward lower frequency was observed upon TiO<sub>2</sub> additions up to 8 mol%. The weak variations in the <sup>29</sup>Si  
 398 MAS spectra can be quantified by measuring the deviation from a Gaussian model lineshape which  
 399 accounts for the spectrum acquired from the TiO<sub>2</sub>-free silica glass ( $\delta_{iso} = -110$  ppm, fwhm=12.3), as

400 illustrated in Figure 7-b. Since  $^{17}\text{O}$  NMR results indicate the formation of Si-O-Ti bonds, it shows that the  
 401  $^{29}\text{Si}$  isotropic chemical shift is almost unchanged by the substitution of  $\text{Si}^{4+}$  by  $\text{Ti}^{4+}$  in the second  
 402 coordination sphere of  $\text{Q}^4$  units. This contrasts with the substitution of a silicon atom by a four-fold  
 403 coordinated  $\text{Al}^{3+}$  or with the formation of a non-bridging oxygen atom, which lead to chemical shift  
 404 variations of 5 and 10 ppm respectively [100]. The trend is confirmed by GIPAW computations of the MD  
 405 amorphous models with 10 mol% of  $\text{TiO}_2$ , which allow to benchmark the  $^{29}\text{Si}$  chemical shift ranges of Si-  
 406  $(\text{OSi})_4$  and  $\text{Si}-(\text{OSi})_3(\text{OTi})$  moieties in a fully-polymerized network of  $\text{SiO}_4$  and  $\text{TiO}_4$  tetrahedra. Indeed, the  
 407  $^{29}\text{Si}$  chemical shift ranges calculated for these two environments are found to overlap completely, with a  
 408 difference of less than 0.7 ppm between their mean chemical shift values (Figure 7-c) and in good agreement  
 409 with former computations of  $^{29}\text{Si}$  chemical shifts in Ti-bearing zeolites (Ricchiardi and Sauer, 1999). In line  
 410 with  $^{17}\text{O}$  NMR results, the  $^{29}\text{Si}$  MAS spectra thus suggest the formation of Si-O-Ti linkages with  
 411 incorporation of titanium atoms as  $\text{TiO}_4$  tetrahedral units in a fully polymerized network up to  $\sim 8$ -10 mol%  
 412  $\text{TiO}_2$ .  
 413



414  
 415 Figure 7. (a)  $^{29}\text{Si}$  MAS NMR spectra of melt-quenched samples recorded at 7.0 T with a spinning rate of  
 416 10 kHz. Experimental spectra are shown in blue, while red dashed lines correspond to the best fit of the  
 417 T0m spectrum with a Gaussian lineshape. (b) Percentage of difference between the experimental spectra

418 and the simulated spectrum of T0m (red circle, left axis) and position of the center of gravity of each  
419 spectrum (blue square, right axis). (c)  $^{29}\text{Si}$  isotropic chemical shift distributions of  $\text{Si}(\text{OSi})_4$  and  
420  $\text{Si}(\text{OSi})_3(\text{OTi})$  environments obtained from GIPAW calculations for the MD models with 10 mol%  $\text{TiO}_2$ .  
421 Average isotropic chemical shifts (and standard deviations) are -112.7 (6.9) and -113.4 (5.6) ppm for  
422  $\text{Si}(\text{OSi})_4$  and  $\text{Si}(\text{OSi})_3(\text{OTi})$ , respectively.

423

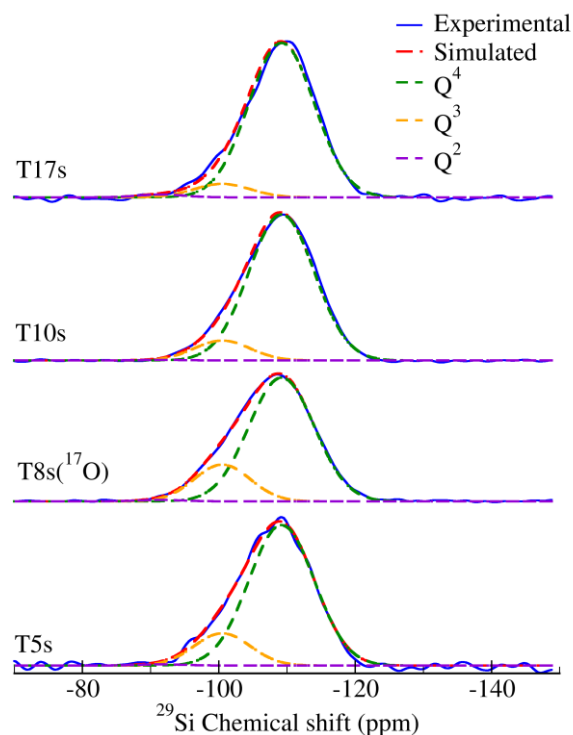
### 424 3.2.2 Sol-gel samples

425 As in the case of melt-quenched glasses, the nature of  $\text{Ti}^{4+}$  incorporation in gel-derived glasses was  
426 studied by  $^{17}\text{O}$  NMR. The  $^{17}\text{O}$  MAS spectrum of the gel-derived glass T8s( $^{17}\text{O}$ ) showed, in addition to the  
427 previously observed O\_2Si and O\_1Si-1Ti signals, a third contribution at lower chemical shift partially  
428 overlapping with the O\_2Si CT peak (Figure 5). This new resonance located at 4.0 ppm could be selectively  
429 highlighted using  $^1\text{H}$ -magnetization transfer experiments, revealing a short O-H distance and being  
430 therefore assigned to O\_1Si-1H moieties in agreement with previous works [106,107]. A small variation of  
431 the  $^{17}\text{O}$  isotropic chemical shift of bridging O\_2Si ( $\delta_{\text{iso}} = 43.1$  ppm,  $C_Q = 5.19$  MHz) is also observed with  
432 respect to the melt-quenched glass. The spectrum did not show any additional signal characteristic of Ti-  
433 O-Ti bonding, suggesting a homogeneous distribution of Ti atoms. Quantitative analysis of the spectrum  
434 gives relative proportions of 89, 7 and 4 % for bridging O\_2Si, O\_1Si-1Ti and non-bridging O\_1Si-1H  
435 oxygen atoms, respectively. The proportion of O\_1Si-1Ti is lower than expected from nominal  
436 composition, which could be associated to a preferential  $^{17}\text{O}$ -enrichment of Si-O-Si linkages since TEOS  
437 was hydrolyzed separately with  $^{17}\text{O}$ -enriched water during synthesis.

438 The  $^{29}\text{Si}$  MAS NMR spectra of the gel-derived samples calcined at  $600^\circ\text{C}$  (Figure 8) showed  
439 obvious differences from those of melt-quenched glasses, with shoulders appearing at higher chemical  
440 shifts associated to depolymerized  $\text{SiO}_4$  units. Indeed,  $^1\text{H}$ - $^{29}\text{Si}$  cross-polarization MAS spectra recorded at  
441 different contact times highlighted the presence of three distinct contributions located at -109.2, -100.5 and  
442 -91.5 ppm (see Figure Sup3). According to  $^{29}\text{Si}$  chemical shift ranges, the peak at -109.2 ppm is assigned  
443 to both  $\text{Si}(\text{OSi})_4$  and  $\text{Si}(\text{OSi})_3(\text{OTi})$   $\text{Q}^4$  units, while the line at -100.5 ppm is assigned to  $\text{Si}(\text{OSi})_3(\text{OH})$   $\text{Q}^3$   
444 units and the later one of much weaker intensity to  $\text{Si}(\text{OSi})_2(\text{OH})_2$   $\text{Q}^2$  moieties. Simulations of quantitative  
445 spectra were done using the parameters extracted from CP MAS spectra and only the intensity of each  
446 component was varied. The position of the  $\text{Q}^4$  line is found very similar with that observed for melt-  
447 quenched samples and the proportion of  $\text{Q}^2$  moieties bearing two hydroxyl groups does not exceed 1% for  
448 all compositions heated at  $600^\circ\text{C}$ . A significant decrease of the relative proportion of  $\text{Q}^3$  units is observed  
449 as the titanium content increases. For the T8s( $^{17}\text{O}$ ) sample, the amount of non-bridging oxygen atoms  
450 determined from the relative intensities of  $\text{Q}^n$  resonances is about 10 %. This corresponds to about twice  
451 the value obtained from the  $^{17}\text{O}$  spectrum (4 %) suggesting a non-uniform  $^{17}\text{O}$ -enrichment of the different

452 bonding environments in the T8s(<sup>17</sup>O) sample. Apart from manifesting OH-bearing structural units, the  
453 <sup>29</sup>Si and <sup>17</sup>O spectra of gel-derived glasses show strong similarities with those of melt-quenched samples  
454 and remain consistent with the incorporation of four-fold coordinated Ti atoms in the silicate network at  
455 low TiO<sub>2</sub> content.

456

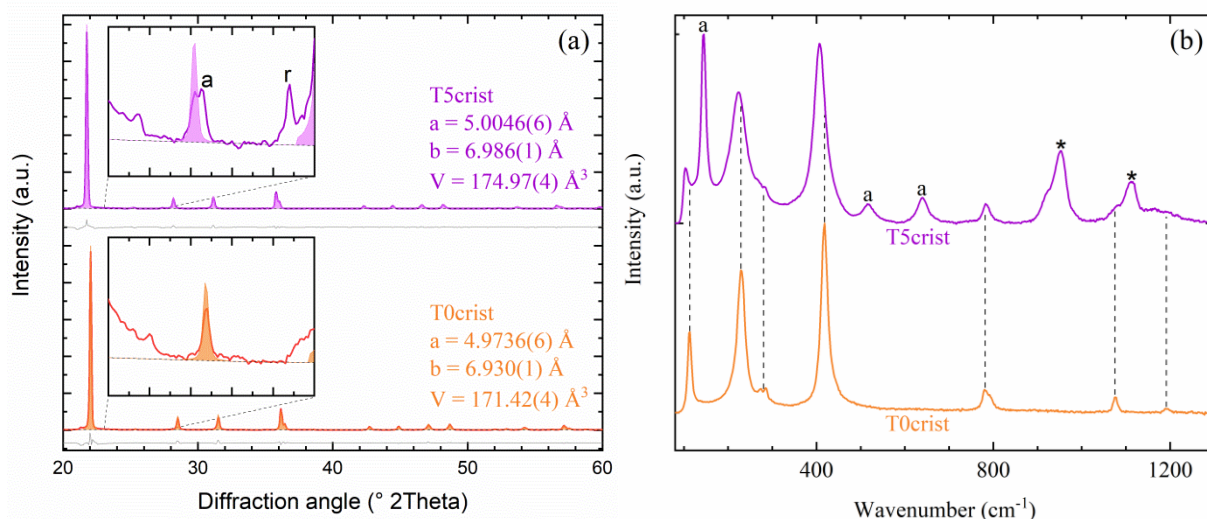


457  
458 Figure 8. Experimental <sup>29</sup>Si NMR spectra of sol-gel samples (blue) and their simulations (dashed red). The  
459 individual Gaussian contributions associated to Q<sup>4</sup>, Q<sup>3</sup> and Q<sup>2</sup> species are shown as dashed green, yellow  
460 and purple, respectively.

461

### 462 3.3 TiO<sub>2</sub>-doped cristobalite

463 To support our discussion of SiO<sub>2</sub>-TiO<sub>2</sub> glasses, we additionally synthesized TiO<sub>2</sub>-doped  
464 cristobalite (sample T5crist) according to the devitrification method reported by previous authors [33]. The  
465 lattice parameters obtained from Le-Bail refinements of XRD data (Fig. 9) confirmed an expansion of the  
466 unit cell of cristobalite upon incorporation of Ti<sup>4+</sup>, due to its larger effective ionic radius (0.42 Å) compared  
467 to Si<sup>4+</sup> (0.26 Å) [105]; anatase and rutile were limited to trace levels in the sample. The Raman spectrum of  
468 T5crist resembled closely that of T0crist, excluding the bands assignable to an anatase impurity;  
469 nevertheless, two additional vibrational features could be discerned at high wavenumber, with maxima  
470 respectively at 955 cm<sup>-1</sup> and 1115 cm<sup>-1</sup>.



471  
 472 Figure 9. Results of the analytical characterization of samples T0cris and T5cris, devitrified respectively  
 473 at 1600 °C and 1450 °C to form cristobalite. a) XRD patterns and related Le-Bail fits, detailing the lattice  
 474 parameters obtained for cristobalite (filled areas: calculated intensity; broken line: background; gray line:  
 475 fit residuals; *a* and *r* label the most intense peak of anatase and rutile, respectively); b) Raman spectra of  
 476 the same samples (labels: *a* for anatase, \* for Raman bands absent in the reference spectrum of tetragonal  
 477 cristobalite [RRUFF-ID: X050046], to which all unmarked features can otherwise be related).

478  
 479 **4. Discussion**

480 The results of our study provide a self-consistent structural view on the formation of glasses in the  
 481 binary system SiO<sub>2</sub>-TiO<sub>2</sub>. Anhydrous glasses can be obtained by melt-quenching at least up to 10 mol%  
 482 TiO<sub>2</sub>, despite the higher difficulty in quenching a homogeneously amorphous material as TiO<sub>2</sub> content  
 483 increases. This observation is consistent with the available phase diagram [21,23], whose eutectic locates  
 484 at ~8 mol%: beyond this point, the first phase predicted to form during cooling through the liquidus is rutile,  
 485 whose ability to precipitate homogeneously in the volume can clearly affect glass-forming ability more than  
 486 cristobalite, which is typically found at the surface. Moreover, the threshold of 10 mol% TiO<sub>2</sub> corresponds  
 487 to the statistical emergence of Ti-O-Ti bonds in a random network of tetrahedral units (the most consistent  
 488 structural description of SiO<sub>2</sub>-TiO<sub>2</sub> glasses, see also below), as mirrored by the average values of our MD  
 489 models in Tab. Sup2. In other words, the statistical presence of Ti-O-Ti direct linkages in the melt appears  
 490 to be energetically unfavorable for glass formation (as supported by the energy differences between various  
 491 relaxed MD models listed in Tab. Sup2), possibly representing the main structural driving force for the  
 492 onset of crystal nucleation.

493 Concerning gel-derived glasses, we analyzed only materials up to 17 mol% TiO<sub>2</sub>, since samples  
494 with 25 mol% and 50 mol% already exhibited crystalline features after the first calcination at 600 °C (SI,  
495 Fig. Sup2). Other authors reported the synthesis of gels of high TiO<sub>2</sub> content and similarly noted their high  
496 instability [40,41,44,48,56,57,59,108–110]. The predictable H<sub>2</sub>O content of our samples, which can be  
497 roughly estimated as a few wt% based on our Raman [93] and <sup>29</sup>Si NMR spectra, persisted even after a pre-  
498 emptive drying stage at 600 °C, so that these materials should be consistently described as belonging to a  
499 ternary compositional system, i.e. SiO<sub>2</sub>-TiO<sub>2</sub>-H<sub>2</sub>O. Obtaining dry glasses from these hydrous gels proved  
500 then rather challenging, probably also due to the lowering of viscosity and to the enhancement of nucleation  
501 usually noticed in water-bearing silicate melts [111–113]. Our observations therefore confirm the  
502 conclusions previously inferred from other compositional systems [114]: the sol-gel route does not seem to  
503 significantly enlarge the anhydrous glass-forming ability of reluctant glass-formers, due to the inevitable  
504 competition between dehydration and devitrification on the way to a fully densified glass. This scenario is  
505 in line with the updated definition of the glassy state of matter and its ultimate fate to crystallize [115],  
506 which disallow a spontaneous glass-to-crystal transformation. As for the observed formation of Ti-rich  
507 pseudo-metallic noduli in T8m(<sup>17</sup>O) during melting at 1800 °C in vacuum, it was clearly caused by the  
508 extreme reducing conditions, which were previously shown to even possibly lead to volatilization of silicon  
509 as gaseous SiO [116]. Notice that the non-detection of these pseudo-metallic noduli on the oxygen spectrum  
510 (expected in the O<sub>2</sub>Ti range) can be explained by their low volume fraction, their minor oxygen content  
511 and also the short recycling delay used in the measurements, optimized for amorphous signals.

512 The computational prediction and experimental confirmation of the absence of an observable and  
513 quantifiable effect of Ti-O-Si bonding on the <sup>29</sup>Si NMR spectra of amorphous materials qualifies again the  
514 characterization of SiO<sub>2</sub>-TiO<sub>2</sub> glasses as a challenging task. Yet, our data obtained from melt-quenched  
515 glasses corroborate full polymerization of the silicate network (only Q<sup>4</sup> species on the <sup>29</sup>Si spectra) upon  
516 actual incorporation of Ti in their structure; Si-O-Ti bonds are moreover clearly observable in the <sup>17</sup>O  
517 spectrum of T8m(<sup>17</sup>O) (despite its partial crystallization). Relating these observations, Ti<sup>4+</sup> must be  
518 isomorphously integrated into the silicate network, as previously proposed by various authors assuming a  
519 prevalent tetrahedral coordination for Ti<sup>4+</sup> (at least at low TiO<sub>2</sub> content) in anhydrous and homogeneous  
520 SiO<sub>2</sub>-TiO<sub>2</sub> glasses [27,28,34,35]. This conclusion is supported by the synthesis of Ti<sup>4+</sup>-containing  
521 cristobalite, in which the transition metal necessarily substitutes Si<sup>4+</sup> in the tetrahedral network sites. The  
522 Raman spectrum of this phase also exhibits two supplementary bands at 955 cm<sup>-1</sup> and 1115 cm<sup>-1</sup>, whose  
523 position is close to that of T<sub>2</sub> and T<sub>3</sub> in glasses, clearly supporting their assignment to the vibrational features  
524 of bridging oxygens related to a 4-coordinated network-forming Ti<sup>4+</sup>; this assignment agrees with the  
525 majority of literature sources [27,29,30,32,117].

526           Regarding the Raman band  $T_1$ , its assignment is less straightforward: given its vicinity to the  
527 position of bands arising in most of the known  $\text{TiO}_2$  polymorphs in the range 600-670  $\text{cm}^{-1}$  [94,118,119],  
528 its interpretation as the signature for 6-coordinated  $\text{Ti}^{4+}$  species in the amorphous network is particularly  
529 tempting, as also claimed by previous authors [27]. This assignment would however imply the formation  
530 of 6-fold  $\text{Ti}^{4+}$  already at very low  $\text{TiO}_2$  content (see the linear dependence from composition observed in  
531 Fig. 2-b), which is in clear antithesis with our MD simulations, NMR data and previous XAS investigations  
532 exhibiting no significant detection of 6-fold  $\text{Ti}^{4+}$  up to at least ~6 mol%  $\text{TiO}_2$  [34,35]. Consequently, the  
533 Raman band may indeed originate from a 6-fold coordinated  $\text{Ti}^{4+}$  content at impurity level, made detectable  
534 due to the especially high Raman sensitivity of these species as compared to other techniques (the high  
535 scattering power of  $\text{TiO}_2$  polymorphs is well known to Raman users); nevertheless, the vibrational feature  
536 could equally stem from an additional mode related to tetrahedrally coordinated  $\text{Ti}^{4+}$ , shifted from the  
537 typical positions observed in  $\text{SiO}_2$  (e.g. the band  $S_4$ ) or in  $\text{GeO}_2$  [86].

538           Based on our data, we also do not find significant reasons for assigning  $\text{Ti}^{4+}$  to a 5-fold oxygen  
539 coordination, which was proposed to be the dominant configuration in gel-derived and partially crystallized  
540  $\text{SiO}_2$ - $\text{TiO}_2$  glasses investigated by other authors [55]. Indeed, MD simulations produce structural models in  
541 which  $\text{Ti}^{4+}$  is invariably 4-fold coordinated. In addition, the presence of  $\text{TiO}_5$  units is expected to lead to  
542 extra-coordinated (3-fold) oxygen atoms with higher chemical shift values, which can be excluded from  
543 the analyses of the  $^{17}\text{O}$  NMR spectra. For the same reason, pronounced clustering of octahedrally  
544 coordinated  $\text{Ti}^{4+}$  in the amorphous state seems also unlikely, since no signal is detected around 600ppm on  
545  $^{17}\text{O}$  spectra. Moreover, pure  $\text{TiO}_2$  has virtually no glass-forming ability and no other vibrational features  
546 are observed at lower wavenumber (100-300  $\text{cm}^{-1}$ ), where the most intense bands of  $\text{TiO}_2$  crystals are  
547 typically found [94,118,119].

548           NMR data obtained from  $\text{H}_2\text{O}$ -bearing gel-derived glasses still revealed the presence of  $\text{Q}^3$  species  
549 ( $^{29}\text{Si}$  spectra) and of Si-OH linkages ( $^{17}\text{O}$  spectra), demonstrating an incomplete dehydration/densification  
550 of their network even after a treatment at 600 °C for 12 h. The lower fraction of  $\text{Q}^3$  species noticed in  $\text{TiO}_2$ -  
551 richer glasses could reflect the expected lower viscosity of these materials, allowing higher structural  
552 mobility and faster  $\text{H}_2\text{O}$  removal during the drying stages: a calorimetric effect interpretable as a glass  
553 transition was observed in T17s at ~675 °C [9], while the  $T_g$  of anhydrous T10m was previously estimated  
554 as ~1000 °C [7] and that of anhydrous  $\text{SiO}_2$  as ~1200 °C [120]. More generally, water incorporation is  
555 likely to represent the crucial factor for the increased glass forming ability of hydrous  $\text{SiO}_2$ - $\text{TiO}_2$  glasses  
556 or, differently formulated, for the higher solubility of  $\text{Ti}^{4+}$  in gel-derived water-bearing silicate glasses: a  
557 partially depolymerized, less rigid network can probably more easily accommodate network distortions due  
558 to the substitution of  $\text{Si}^{4+}$  for the substantially larger  $\text{Ti}^{4+}$ , also avoiding energetically less favorable Ti-O-  
559 Ti direct linkages.

560

561 **5. Conclusion**

562 We used a combination of Raman spectroscopy, molecular dynamics, GIPAW computations and  
563 solid-state  $^{29}\text{Si}$  and  $^{17}\text{O}$  NMR as a powerful multipronged approach for the structural characterization of  
564 glasses. Taking into account all hypotheses proposed in the literature, we have been able to confirm that  
565 titanium prevalently assumes a tetrahedral oxygen coordination in anhydrous  $\text{SiO}_2\text{-TiO}_2$  glasses and that  
566 the glass solubility of  $\text{TiO}_2$  is limited to  $\sim 10$  mol%. Gel-derived glasses can incorporate substantially higher  
567 amounts of  $\text{TiO}_2$ , most likely due to the depolymerizing effect of a non-negligible water content: this result  
568 suggests that dehydration may be crucial in driving the crystallization of transition metal oxides in melts.  
569 All in all, the sol-gel route does not appear a viable solution for enlarging the glass-forming range of  
570 anhydrous silicates.

571

572 **Acknowledgements**

573 A.Z. wishes to acknowledge the Deutsche Forschungsgemeinschaft (DFG) for funding his research  
574 through the Walter Benjamin Program, grant no. ZA 1188/1-1. Also J.D. and G.H. acknowledge the support  
575 of DFG, grant no. DE 598/33-1. The authors are additionally grateful to: (i) Vinzent Olszok and Prof. Alfred  
576 P. Weber, for the assistance during the synthesis of spray-dried nanobeads at the Institute of Particle  
577 Technology at TU Clausthal; (ii) the ICMN laboratory (Orléans, France) for TEM access and Dr. Cécile  
578 Genevois as an operator; (iii) the French Agency for Research for its financial support through the Equipex  
579 Planex ANR-11-EQPX-36; (iv) the TGIR-RMN-THC Fr3050 CNRS for its financial support and (v) the  
580 CaSciModOT project (Calcul Scientifique et la Modélisation à Orléans et Tours) for the access to high  
581 performance computing facilities.

582 **References**

- 583 [1] F.J. Ryerson, E.B. Watson, Rutile saturation in magmas: implications for TiNbTa depletion in  
584 island-arc basalts, *Earth and Planetary Science Letters*. 86 (1987) 225–239.  
585 [https://doi.org/10.1016/0012-821X\(87\)90223-8](https://doi.org/10.1016/0012-821X(87)90223-8).
- 586 [2] G.A. Gaetani, P.D. Asimow, E.M. Stolper, A model for rutile saturation in silicate melts with  
587 applications to eclogite partial melting in subduction zones and mantle plumes, *Earth and Planetary*  
588 *Science Letters*. 272 (2008) 720–729. <https://doi.org/10.1016/j.epsl.2008.06.002>.
- 589 [3] K. Kularatne, A. Audétat, Rutile solubility in hydrous rhyolite melts at 750–900°C and 2kbar, with  
590 application to titanium-in-quartz (TitaniQ) thermobarometry, *Geochimica et Cosmochimica Acta*.  
591 125 (2014) 196–209. <https://doi.org/10.1016/j.gca.2013.10.020>.
- 592 [4] F.P. Leitzke, R.O.C. Fonseca, J. Göttlicher, R. Steininger, S. Jahn, C. Prescher, M. Lagos, Ti K-edge  
593 XANES study on the coordination number and oxidation state of Titanium in pyroxene, olivine,  
594 armalcolite, ilmenite, and silicate glass during mare basalt petrogenesis, *Contrib Mineral Petrol*. 173  
595 (2018) 103. <https://doi.org/10.1007/s00410-018-1533-7>.
- 596 [5] D. Di Genova, R.A. Brooker, H.M. Mader, J.W.E. Drewitt, A. Longo, J. Deubener, D.R. Neuville,  
597 S. Fanara, O. Shebanova, S. Anzellini, F. Arzilli, E.C. Bamber, L. Hennet, G. La Spina, N. Miyajima,  
598 In situ observation of nanolite growth in volcanic melt: A driving force for explosive eruptions,  
599 *Science Advances*. 6 (2020). <https://doi.org/10.1126/sciadv.abb0413>.
- 600 [6] W. Höland, G.H. Beall, Principles of Designing Glass-Ceramic Formation, in: *Glass-Ceramic*  
601 *Technology*, John Wiley & Sons, Ltd, 2019: pp. 1–66. <https://doi.org/10.1002/9781119423737.ch1>.
- 602 [7] P.C. Schultz, Binary Titania-Silica Glasses Containing 10 to 20 Wt% TiO<sub>2</sub>, *Journal of the American*  
603 *Ceramic Society*. 59 (1976) 214–219. <https://doi.org/10.1111/j.1151-2916.1976.tb10936.x>.
- 604 [8] A. Baiker, P. Dollenmeier, M. Glinski, A. Reller, Selective catalytic reduction of nitric oxide with  
605 ammonia: II. Monolayers of Vanadia Immobilized on Titania—Silica Mixed Gels, *Applied*  
606 *Catalysis*. 35 (1987) 365–380. [https://doi.org/10.1016/S0166-9834\(00\)82873-0](https://doi.org/10.1016/S0166-9834(00)82873-0).
- 607 [9] A. Zandona, A. Martínez Arias, M. Gutbrod, G. Hensch, A.P. Weber, J. Deubener, Spray-Dried  
608 TiO<sub>2</sub>(B)-Containing Photocatalytic Glass-Ceramic Nanobeads, *Adv. Funct. Mater.* (2020) 2007760.  
609 <https://doi.org/10.1002/adfm.202007760>.
- 610 [10] A. Dietzel, Die Kationenfeldstärken und ihre Beziehungen zu Entglasungsvorgängen, zur  
611 Verbindungsbildung und zu den Schmelzpunkten von Silicaten, *Zeitschrift Für Elektrochemie Und*  
612 *Angewandte Physikalische Chemie*. 48 (1942) 9–23. <https://doi.org/10.1002/bbpc.19420480104>.
- 613 [11] D.B. Dingwell, E. Paris, F. Seifert, A. Mottana, C. Romano, X-ray absorption study of Ti-bearing  
614 silicate glasses, *Phys Chem Minerals*. 21 (1994). <https://doi.org/10.1007/BF00203924>.
- 615 [12] F. Farges, G.E. Brown, A. Navrotsky, H. Gan, J.J. Rehr, Coordination chemistry of Ti(IV) in silicate  
616 glasses and melts: II. Glasses at ambient temperature and pressure, *Geochimica et Cosmochimica*  
617 *Acta*. 60 (1996) 3039–3053. [https://doi.org/10.1016/0016-7037\(96\)00145-7](https://doi.org/10.1016/0016-7037(96)00145-7).
- 618 [13] F. Farges, G.E. Brown, A. Navrotsky, H. Gan, J.R. Rehr, Coordination chemistry of Ti(IV) in silicate  
619 glasses and melts: III. Glasses and melts from ambient to high temperatures, *Geochimica et*  
620 *Cosmochimica Acta*. 60 (1996) 3055–3065. [https://doi.org/10.1016/0016-7037\(96\)00146-9](https://doi.org/10.1016/0016-7037(96)00146-9).
- 621 [14] C. Romano, E. Paris, B.T. Poe, G. Giuli, D.B. Dingwell, A. Mottana, Effect of aluminum on Ti-  
622 coordination in silicate glasses: A XANES study, *American Mineralogist*. 85 (2000) 108–117.  
623 <https://doi.org/10.2138/am-2000-0112>.
- 624 [15] G.S. Henderson, X. Liu, M.E. Fleet, A Ti L-edge X-ray absorption study of Ti-silicate glasses,  
625 *Physics and Chemistry of Minerals*. 29 (2002) 32–42. <https://doi.org/10.1007/s002690100208>.
- 626 [16] E.T. Nienhuis, J. Marcial, T. Robine, C. Le Losq, D.R. Neuville, M.C. Stennett, N.C. Hyatt, J.S.  
627 McCloy, Effect of Ti<sup>4+</sup> on the structure of nepheline (NaAlSiO<sub>4</sub>) glass, *Geochimica et*  
628 *Cosmochimica Acta*. 290 (2020) 333–351. <https://doi.org/10.1016/j.gca.2020.09.015>.
- 629 [17] F. Farges, G.E. Brown, J.J. Rehr, Coordination chemistry of Ti(IV) in silicate glasses and melts: I.  
630 XAFS study of titanium coordination in oxide model compounds, *Geochimica et Cosmochimica*  
631 *Acta*. 60 (1996) 3023–3038. [https://doi.org/10.1016/0016-7037\(96\)00144-5](https://doi.org/10.1016/0016-7037(96)00144-5).

- 632 [18] F. Farges, G.E. Brown, Coordination chemistry of titanium (IV) in silicate glasses and melts: IV.  
633 XANES studies of synthetic and natural volcanic glasses and tektites at ambient temperature and  
634 pressure, *Geochimica et Cosmochimica Acta*. 61 (1997) 1863–1870. [https://doi.org/10.1016/S0016-](https://doi.org/10.1016/S0016-7037(97)00050-1)  
635 7037(97)00050-1.
- 636 [19] L. Cormier, O. Dargaud, N. Menguy, G.S. Henderson, M. Guignard, N. Trcera, B. Watts,  
637 Investigation of the Role of Nucleating Agents in MgO–SiO<sub>2</sub>–Al<sub>2</sub>O<sub>3</sub>–SiO<sub>2</sub>–TiO<sub>2</sub> Glasses and  
638 Glass-Ceramics: A XANES Study at the Ti K- and L<sub>2,3</sub>-Edges, *Crystal Growth & Design*. 11 (2011)  
639 311–319. <https://doi.org/10.1021/cg101318p>.
- 640 [20] D.L. Evans, Glass structure: The bridge between the molten and crystalline states, *Journal of Non-*  
641 *Crystalline Solids*. 52 (1982) 115–128. [https://doi.org/10.1016/0022-3093\(82\)90285-X](https://doi.org/10.1016/0022-3093(82)90285-X).
- 642 [21] E.N. Bunting, Phase equilibria in the systems TiO<sub>2</sub>, TiO<sub>2</sub>-SiO<sub>2</sub> and TiO<sub>2</sub>-Al<sub>2</sub>O<sub>3</sub>, *BUR. STAN. J.*  
643 *RES.* 11 (1933) 719. <https://doi.org/10.6028/jres.011.049>.
- 644 [22] R.W. Ricker, F.A. Hummel, Reactions in the System TiO<sub>2</sub>-SiO<sub>2</sub>; Revision of the Phase Diagram, *J*  
645 *American Ceramic Society*. 34 (1951) 271–279. [https://doi.org/10.1111/j.1151-](https://doi.org/10.1111/j.1151-2916.1951.tb09129.x)  
646 2916.1951.tb09129.x.
- 647 [23] R.C. DeVries, R. Roy, E.F. Osborn, Phase Equilibria in the System CaO-TiO<sub>2</sub>-SiO<sub>2</sub>, *Journal of The*  
648 *American Ceramic Society*. 38 (1955) 158–171.
- 649 [24] S.A. Kirillova, V.I. Almjashv, V.V. Gusarov, Phase Relationships in the SiO<sub>2</sub>-TiO<sub>2</sub> System, 56  
650 (2011) 9.
- 651 [25] C. Zhang, X. Ge, Q. Hu, F. Yang, P. Lai, C. Shi, W. Lu, J. Li, Atomic scale structural analysis of  
652 liquid immiscibility in binary silicate melt: A case of SiO<sub>2</sub>-TiO<sub>2</sub> system, *Journal of Materials*  
653 *Science & Technology*. 53 (2020) 53–60.
- 654 [26] D.G. Ostrizhko, G.A. Pavlova, Structure of Glasses in the Silicon Dioxide Titanium Dioxide System,  
655 *Izv. Akad. Nauk SSR, Neorg. Mat.* 6 (1970) 74–77.
- 656 [27] B.G. Varshal, V.N. Denisov, B.N. Mavrin, G.A. Parlova, V.B. Podobedov, Kh.E. Sterin, Spectra of  
657 Raman and hyper-Raman light scattering of the TiO<sub>2</sub>-SiO<sub>2</sub> glass system, *Opt. Spektrosk.* 47 (1979)  
658 619–622.
- 659 [28] P.P. Bihuniak, R.A. Condrate, Structures, spectra and related properties of group IVB-doped  
660 vitreous silica, *Journal of Non-Crystalline Solids*. 44 (1981) 331–343. [https://doi.org/10.1016/0022-](https://doi.org/10.1016/0022-3093(81)90036-3)  
661 3093(81)90036-3.
- 662 [29] K. Kusabiraki, Infrared and raman spectra of vitreous silica and sodium silicates containing titanium,  
663 *Journal of Non-Crystalline Solids*. 95–96 (1987) 411–417. [https://doi.org/10.1016/S0022-](https://doi.org/10.1016/S0022-3093(87)80138-2)  
664 3093(87)80138-2.
- 665 [30] M.C. Tobin, T. Baak, Raman Spectra of Some Low-Expansion Glasses, *J. Opt. Soc. Am.* 58 (1968)  
666 1459. <https://doi.org/10.1364/JOSA.58.001459>.
- 667 [31] C.F. Smith, R.A. Condrate, W.E. Votava, The Difference Infrared Spectra of Titanium-Containing  
668 Vitreous Silica, *Appl Spectrosc.* 29 (1975) 79–81. <https://doi.org/10.1366/000370275774455437>.
- 669 [32] H.R. Chandrasekhar, M. Chandrasekhar, M.H. Manghnani, Phonons in TiO<sub>2</sub>-SiO<sub>2</sub> glasses, *Journal*  
670 *of Non-Crystalline Solids*. 40 (1980) 567–575. [https://doi.org/10.1016/0022-3093\(80\)90130-1](https://doi.org/10.1016/0022-3093(80)90130-1).
- 671 [33] D.L. Evans, Solid Solution of TiO<sub>2</sub> in SiO<sub>2</sub>, *Journal of the American Ceramic Society*. 53 (1970)  
672 418–418. <https://doi.org/10.1111/j.1151-2916.1970.tb12146.x>.
- 673 [34] D.R. Sandstrom, F.W. Lytle, P.S.P. Wei, R.B. Gregor, J. Wong, P. Schultz, Coordination of Ti in  
674 TiO<sub>2</sub>□SiO<sub>2</sub> glass by X-ray absorption spectroscopy, *Journal of Non-Crystalline Solids*. 41 (1980)  
675 201–207. [https://doi.org/10.1016/0022-3093\(80\)90165-9](https://doi.org/10.1016/0022-3093(80)90165-9).
- 676 [35] R.B. Gregor, F.W. Lytle, D.R. Sandstrom, J. Wong, P. Schultz, Investigation of TiO<sub>2</sub>-SiO<sub>2</sub> Glasses  
677 by X-ray absorption spectroscopy, *Journal of Non-Crystalline Solids*. 55 (1983) 27–43.
- 678 [36] S.M. Mukhopadhyay, S.H. Garofalini, Surface studies of TiO<sub>2</sub>-SiO<sub>2</sub> glasses by X-ray  
679 photoelectron spectroscopy, *Journal of Non-Crystalline Solids*. 126 (1990) 202–208.  
680 [https://doi.org/10.1016/0022-3093\(90\)90820-C](https://doi.org/10.1016/0022-3093(90)90820-C).

- 681 [37] A. Chmel, G.M. Eranosyan, A.A. Kharshak, Vibrational spectroscopic study of Ti-substituted SiO<sub>2</sub>,  
682 Journal of Non-Crystalline Solids. 146 (1992) 213–217. [https://doi.org/10.1016/S0022-](https://doi.org/10.1016/S0022-3093(05)80493-4)  
683 3093(05)80493-4.
- 684 [38] S. Richter, D. Möncke, F. Zimmermann, E.I. Kamitsos, L. Wondraczek, A. Tünnermann, S. Nolte,  
685 Ultrashort pulse induced modifications in ULE - from nanograting formation to laser darkening,  
686 Opt. Mater. Express. 5 (2015) 1834–1850. <https://doi.org/10.1364/OME.5.001834>.
- 687 [39] S.C. Cheng, Coordination and optical attenuation of TiO<sub>2</sub>–SiO<sub>2</sub> glass by electron energy loss  
688 spectroscopy, Journal of Non-Crystalline Solids. 354 (2008) 3735–3741.  
689 <https://doi.org/10.1016/j.jnoncrysol.2008.03.045>.
- 690 [40] C.J.R. Gonzalez-Oliver, P.F. James, H. Rawson, Silica and silica-titania glasses prepared by the sol-  
691 gel process, Journal of Non-Crystalline Solids. 48 (1982) 129–152. [https://doi.org/10.1016/0022-](https://doi.org/10.1016/0022-3093(82)90251-4)  
692 3093(82)90251-4.
- 693 [41] T. Hayashi, T. Yamada, H. Saito, Preparation of titania-silica glasses by the gel method, J Mater Sci.  
694 18 (1983) 3137–3142. <https://doi.org/10.1007/BF00700798>.
- 695 [42] M. Emili, L. Incoccia, S. Mobilio, G. Fagherazzi, M. Guglielmi, Structural investigations of TiO<sub>2</sub>-  
696 SiO<sub>2</sub> glassy and glass-ceramic materials prepared by the sol-gel method, Journal of Non-Crystalline  
697 Solids. 74 (1985) 129–146. [https://doi.org/10.1016/0022-3093\(85\)90407-7](https://doi.org/10.1016/0022-3093(85)90407-7).
- 698 [43] M. Schraml-Marth, K.L. Walther, A. Wokaun, B.E. Handy, A. Baiker, Porous silica gels and  
699 TiO<sub>2</sub>/SiO<sub>2</sub> mixed oxides prepared via the sol-gel process: characterization by spectroscopic  
700 techniques, Journal of Non-Crystalline Solids. 143 (1992) 93–111. [https://doi.org/10.1016/S0022-](https://doi.org/10.1016/S0022-3093(05)80557-5)  
701 3093(05)80557-5.
- 702 [44] M. Beghi, P. Chiurlo, L. Costa, M. Palladino, M.F. Pirini, Structural investigation of the silica-titania  
703 gel/glass transition, Journal of Non-Crystalline Solids. 145 (1992) 175–179.  
704 [https://doi.org/10.1016/S0022-3093\(05\)80451-X](https://doi.org/10.1016/S0022-3093(05)80451-X).
- 705 [45] L. Delattre, F. Babonneau, <sup>17</sup>O Solution NMR Characterization of the Preparation of Sol-Gel  
706 Derived SiO<sub>2</sub>/TiO<sub>2</sub> and SiO<sub>2</sub>/ZrO<sub>2</sub> Glasses, Chem. Mater. 9 (1997) 2385–2394.  
707 <https://doi.org/10.1021/cm970372f>.
- 708 [46] C. Gervais, F. Babonneau, M.E. Smith, Detection, Quantification, and Magnetic Field Dependence  
709 of Solid-State <sup>17</sup>O NMR of X–O–Y (X,Y = Si,Ti) Linkages: Implications for Characterizing  
710 Amorphous Titania-Silica-Based Materials, J. Phys. Chem. B. 105 (2001) 1971–1977.  
711 <https://doi.org/10.1021/jp003519q>.
- 712 [47] D.S. Knight, C.G. Pantano, W.B. White, Raman spectra of gel-prepared titania-silica glasses,  
713 Materials Letters. 8 (1989) 156–160. [https://doi.org/10.1016/0167-577X\(89\)90182-1](https://doi.org/10.1016/0167-577X(89)90182-1).
- 714 [48] I.M.M. Salvado, J.M.F. Navarro, Phase separation in materials of the systems TiO<sub>2</sub>-SiO<sub>2</sub> and ZrO<sub>2</sub>-  
715 SiO<sub>2</sub> prepared by the alkoxide route, Journal of Materials Science Letters. 9 (1990) 173–176.  
716 <https://doi.org/10.1007/BF00727707>.
- 717 [49] R. Puyané, P.F. James, H. Rawson, Preparation of silica and soda-silica glasses by the sol-gel  
718 process, Journal of Non-Crystalline Solids. 41 (1980) 105–115. [https://doi.org/10.1016/0022-](https://doi.org/10.1016/0022-3093(80)90196-9)  
719 3093(80)90196-9.
- 720 [50] A. Bertoluzza, C. Fagnano, M. Antonietta Morelli, V. Gottardi, M. Guglielmi, Raman and infrared  
721 spectra on silica gel evolving toward glass, Journal of Non-Crystalline Solids. 48 (1982) 117–128.  
722 [https://doi.org/10.1016/0022-3093\(82\)90250-2](https://doi.org/10.1016/0022-3093(82)90250-2).
- 723 [51] L.C. Klein, T.A. Gallo, G.J. Garvey, Densification of monolithic silica gels below 1000°C, Journal  
724 of Non-Crystalline Solids. 63 (1984) 23–33. [https://doi.org/10.1016/0022-3093\(84\)90383-1](https://doi.org/10.1016/0022-3093(84)90383-1).
- 725 [52] T.A. Gallo, L.C. Klein, Apparent viscosity of sol-gel processed silica, Journal of Non-Crystalline  
726 Solids. 82 (1986) 198–204. [https://doi.org/10.1016/0022-3093\(86\)90131-6](https://doi.org/10.1016/0022-3093(86)90131-6).
- 727 [53] G.S. Henderson, M.E. Fleet, The structure of Ti silicate glasses by micro-Raman spectroscopy, The  
728 Canadian Mineralogist. 33 (1995) 399–408.
- 729 [54] G.S. Henderson, M.E. Fleet, The structure of titanium silicate glasses investigated by Si K-edge X-  
730 ray absorption spectroscopy, Journal of Non-Crystalline Solids. 211 (1997) 214–221.  
731 [https://doi.org/10.1016/S0022-3093\(96\)00640-0](https://doi.org/10.1016/S0022-3093(96)00640-0).

- 732 [55] G.S. Henderson, X. Liu, M.E. Fleet, Titanium coordination in silicate glasses investigated using O  
733 K-edge X-ray absorption spectroscopy, *Mineralogical Magazine*. 67 (2003) 597–607.  
734 <https://doi.org/10.1180/0026461036740120>.
- 735 [56] M.E. Smith, H.J. Whitfield, Application of oxygen-17 NMR spectroscopy to detection of atomic  
736 scale phase separation in titania-silica gels, *J. Chem. Soc., Chem. Commun.* (1994) 723.  
737 <https://doi.org/10.1039/c39940000723>.
- 738 [57] P.J. Dirken, M.E. Smith, H.J. Whitfield, <sup>17</sup>O and <sup>29</sup>Si Solid State NMR Study of Atomic Scale  
739 Structure in Sol-Gel-Prepared TiO<sub>2</sub>-SiO<sub>2</sub> Materials, *J. Phys. Chem.* 99 (1995) 395–401.  
740 <https://doi.org/10.1021/j100001a059>.
- 741 [58] J.S. Rigden, J.K. Walters, P.J. Dirken, M.E. Smith, G. Bushnell-Wye, W.S. Howells, R.J. Newport,  
742 The role of titanium in : mixed sol-gels: an x-ray and neutron diffraction study, *J. Phys.: Condens.*  
743 *Matter.* 9 (1997) 4001–4016. <https://doi.org/10.1088/0953-8984/9/20/001>.
- 744 [59] R. Anderson, G. Mountjoy, M.E. Smith, R.J. Newport, An EXAFS study of silica–titania sol–gels,  
745 *Journal of Non-Crystalline Solids*. 232–234 (1998) 72–79. [https://doi.org/10.1016/S0022-3093\(98\)00373-1](https://doi.org/10.1016/S0022-3093(98)00373-1).
- 746 [60] G. Mountjoy, D.M. Pickup, G.W. Wallidge, R. Anderson, J.M. Cole, R.J. Newport, M.E. Smith,  
747 XANES Study of Ti Coordination in Heat-Treated (TiO<sub>2</sub>)<sub>x</sub>(SiO<sub>2</sub>)<sub>1-x</sub> Xerogels, *Chem. Mater.* 11  
748 (1999) 1253–1258. <https://doi.org/10.1021/cm980644u>.
- 749 [61] G. Mountjoy, D.M. Pickup, G.W. Wallidge, J.M. Cole, R.J. Newport, M.E. Smith, In-situ high-  
750 temperature XANES observations of rapid and reversible changes in Ti coordination in titania–silica  
751 xerogels, *Chemical Physics Letters*. 304 (1999) 150–154. [https://doi.org/10.1016/S0009-2614\(99\)00302-4](https://doi.org/10.1016/S0009-2614(99)00302-4).
- 752 [62] D.M. Pickup, F.E. Sowrey, R.J. Newport, P.N. Gunawidjaja, K.O. Drake, M.E. Smith, The Structure  
753 of TiO<sub>2</sub>–SiO<sub>2</sub> Sol–Gel Glasses from Neutron Diffraction with Isotopic Substitution of Titanium  
754 and <sup>17</sup>O and <sup>49</sup>Ti Solid-State NMR with Isotopic Enrichment, *J. Phys. Chem. B*. 108 (2004) 10872–  
755 10880. <https://doi.org/10.1021/jp049053j>.
- 756 [63] G.W. Wallidge, R. Anderson, G. Mountjoy, D.M. Pickup, P. Gunawidjaja, R.J. Newport, M.E.  
757 Smith, Advanced physical characterisation of the structural evolution of amorphous  
758 (TiO<sub>2</sub>)<sub>x</sub>(SiO<sub>2</sub>)<sub>1-x</sub>sol-gel materials, *Journal of Materials Science*. 39 (2004) 6743–6755.  
759 <https://doi.org/10.1023/B:JMSC.0000045604.02983.96>.
- 760 [64] A. Zandonà, M. Moustrous, C. Genevois, E. Véron, A. Canizarès, M. Allix, Glass-forming ability  
761 and ZrO<sub>2</sub> saturation limits in the magnesium aluminosilicate system, *Ceramics International*. (2021).  
762 <https://doi.org/10.1016/j.ceramint.2021.12.051>.
- 763 [65] Leo. Brewer, Thermodynamic Properties of the Oxides and their Vaporization Processes., *Chem.*  
764 *Rev.* 52 (1953) 1–75. <https://doi.org/10.1021/cr60161a001>.
- 765 [66] B. Lafuente, R.T. Downs, H. Yang, N. Stone, 1. The power of databases: The RRUFF project, in:  
766 *Highlights in Mineralogical Crystallography*, De Gruyter, Berlin, Boston, 2015: pp. 1–30.  
767 <https://doi.org/10.1515/9783110417104-003>.
- 768 [67] I.T. Todorov, W. Smith, K. Trachenko, M.T. Dove, DL\_POLY\_3: new dimensions in molecular  
769 dynamics simulations via massive parallelism, *J. Mater. Chem.* 16 (2006) 1911–1918.  
770 <https://doi.org/10.1039/B517931A>.
- 771 [68] K. Okhotnikov, B. Stevansson, M. Edén, New interatomic potential parameters for molecular  
772 dynamics simulations of rare-earth (RE = La, Y, Lu, Sc) aluminosilicate glass structures: exploration  
773 of RE<sup>3+</sup> field-strength effects, *Phys. Chem. Chem. Phys.* 15 (2013) 15041–15055.  
774 <https://doi.org/10.1039/C3CP51726H>.
- 775 [69] G. Malavasi, A. Pedone, M.C. Menziani, Towards a quantitative rationalization of multicomponent  
776 glass properties by means of molecular dynamics simulations, *Null*. 32 (2006) 1045–1055.  
777 <https://doi.org/10.1080/08927020600932793>.
- 778 [70] S.J. Clark, M.D. Segall, C.J. Pickard, P.J. Hasnip, M.I.J. Probert, K. Refson, M.C. Payne, First  
779 principles methods using CASTEP, *Zeitschrift Für Kristallographie - Crystalline Materials*. 220  
780 (2005) 567–570. <https://doi.org/doi:10.1524/zkri.220.5.567.65075>.

- 783 [71] C.J. Pickard, F. Mauri, All-electron magnetic response with pseudopotentials: NMR chemical shifts,  
784 Phys. Rev. B. 63 (2001) 245101. <https://doi.org/10.1103/PhysRevB.63.245101>.
- 785 [72] M. Profeta, F. Mauri, C.J. Pickard, Accurate First Principles Prediction of  $^{17}\text{O}$  NMR Parameters in  
786  $\text{SiO}_2$ : Assignment of the Zeolite Ferrierite Spectrum, J. Am. Chem. Soc. 125 (2003) 541–548.  
787 <https://doi.org/10.1021/ja027124r>.
- 788 [73] J.P. Perdew, K. Burke, M. Ernzerhof, Generalized Gradient Approximation Made Simple, Phys.  
789 Rev. Lett. 77 (1996) 3865–3868. <https://doi.org/10.1103/PhysRevLett.77.3865>.
- 790 [74] J.R. Yates, C.J. Pickard, F. Mauri, Calculation of NMR chemical shifts for extended systems using  
791 ultrasoft pseudopotentials, Phys. Rev. B. 76 (2007) 024401.  
792 <https://doi.org/10.1103/PhysRevB.76.024401>.
- 793 [75] S. Cadars, R. Guégan, M.N. Garaga, X. Bourrat, L. Le Forestier, F. Fayon, T.V. Huynh, T. Allier,  
794 Z. Nour, D. Massiot, New Insights into the Molecular Structures, Compositions, and Cation  
795 Distributions in Synthetic and Natural Montmorillonite Clays, Chem. Mater. 24 (2012) 4376–4389.  
796 <https://doi.org/10.1021/cm302549k>.
- 797 [76] J.S. Waugh, Sensitivity in Fourier transform NMR spectroscopy of slowly relaxing systems, Journal  
798 of Molecular Spectroscopy. 35 (1970) 298–305. [https://doi.org/10.1016/0022-2852\(70\)90205-5](https://doi.org/10.1016/0022-2852(70)90205-5).
- 799 [77] F.H. Larsen, I. Farnan,  $^{29}\text{Si}$  and  $^{17}\text{O}$  (Q)CPMG-MAS solid-state NMR experiments as an optimum  
800 approach for half-integer nuclei having long  $T_1$  relaxation times, Chemical Physics Letters. 357  
801 (2002) 403–408. [https://doi.org/10.1016/S0009-2614\(02\)00520-1](https://doi.org/10.1016/S0009-2614(02)00520-1).
- 802 [78] C.A. Fyfe, K.T. Mueller, H. Grondey, K.C. Wong-Moon, Dipolar dephasing between quadrupolar  
803 and spin-12 nuclei. REDOR and TEDOR NMR experiments on VPI-5, Chemical Physics Letters.  
804 199 (1992) 198–204. [https://doi.org/10.1016/0009-2614\(92\)80069-N](https://doi.org/10.1016/0009-2614(92)80069-N).
- 805 [79] J. Trebosc, B. Hu, J.P. Amoureux, Z. Gan, Through-space R3-HETCOR experiments between spin-  
806  $1/2$  and half-integer quadrupolar nuclei in solid-state NMR, Journal of Magnetic Resonance. 186  
807 (2007) 220–227. <https://doi.org/10.1016/j.jmr.2007.02.015>.
- 808 [80] A. Brinkmann, A.P.M. Kentgens, Proton-Selective  $^{17}\text{O}$ -H Distance Measurements in Fast Magic-  
809 Angle-Spinning Solid-State NMR Spectroscopy for the Determination of Hydrogen Bond Lengths,  
810 J. Am. Chem. Soc. 128 (2006) 14758–14759. <https://doi.org/10.1021/ja065415k>.
- 811 [81] R. Giovine, J. Trébosc, F. Pourpoint, O. Lafon, J.-P. Amoureux, Magnetization transfer from protons  
812 to quadrupolar nuclei in solid-state NMR using PRESTO or dipolar-mediated refocused INEPT  
813 methods, Journal of Magnetic Resonance. 299 (2019) 109–123.  
814 <https://doi.org/10.1016/j.jmr.2018.12.016>.
- 815 [82] J.J. Helmus, C.P. Jaroniec, NmrGlue: an open source Python package for the analysis of  
816 multidimensional NMR data, Journal of Biomolecular NMR. 55 (2013) 355–367.  
817 <https://doi.org/10.1007/s10858-013-9718-x>.
- 818 [83] C.R. Harris, K.J. Millman, S.J. van der Walt, R. Gommers, P. Virtanen, D. Cournapeau, E. Wieser,  
819 J. Taylor, S. Berg, N.J. Smith, R. Kern, M. Picus, S. Hoyer, M.H. van Kerkwijk, M. Brett, A.  
820 Haldane, J.F. del Río, M. Wiebe, P. Peterson, P. Gérard-Marchant, K. Sheppard, T. Reddy, W.  
821 Weckesser, H. Abbasi, C. Gohlke, T.E. Oliphant, Array programming with NumPy, Nature. 585  
822 (2020) 357–362. <https://doi.org/10.1038/s41586-020-2649-2>.
- 823 [84] D. Massiot, F. Fayon, M. Capron, I. King, S. Le Calvé, B. Alonso, J.-O. Durand, B. Bujoli, Z. Gan,  
824 G. Hoatson, Modelling one- and two-dimensional solid-state NMR spectra, Magnetic Resonance in  
825 Chemistry. 40 (2002) 70–76. <https://doi.org/10.1002/mrc.984>.
- 826 [85] T. Charpentier, C. Fermon, J. Virlet, Numerical and theoretical analysis of multiquantum magic-  
827 angle spinning experiments, J. Chem. Phys. 109 (1998) 3116–3130.  
828 <https://doi.org/10.1063/1.476903>.
- 829 [86] F.L. Galeener, G. Lucovsky, Longitudinal Optical Vibrations in Glasses:  $\text{GeO}_2$  and  $\text{SiO}_2$ , Phys.  
830 Rev. Lett. 37 (1976) 1474–1478. <https://doi.org/10.1103/PhysRevLett.37.1474>.
- 831 [87] F.L. Galeener, J.C. Mikkelsen, Vibrational dynamics in  $\text{O}^{18}$ -substituted vitreous  $\text{SiO}_2$ , Phys. Rev.  
832 B. 23 (1981) 5527–5530. <https://doi.org/10.1103/PhysRevB.23.5527>.

- 833 [88] F.L. Galeener, A.E. Geissberger, Vibrational dynamics in 30Si-substituted vitreous SiO<sub>2</sub>, *Physical*  
834 *Review B*. 27 (1983) 6199–6204.
- 835 [89] R.A. Barrio, F.L. Galeener, E. Martínez, R.J. Elliott, Regular ring dynamics in AX<sub>2</sub> tetrahedral  
836 glasses, *Phys. Rev. B*. 48 (1993) 15672–15689. <https://doi.org/10.1103/PhysRevB.48.15672>.
- 837 [90] F.L. Galeener, Planar rings in glasses, *Solid State Communications*. 44 (1982) 1037–1040.
- 838 [91] P.F. Mcmillan, B.T. Poe, P. Gillet, B. Reynard, A study of SiO<sub>2</sub> glass and supercooled liquid to  
839 1950 K via high-temperature Raman spectroscopy, *Geochimica et Cosmochimica Acta*. 58 (1994)  
840 3653–3664.
- 841 [92] R.H. Stolen, G.E. Walrafen, Water and its relation to broken bond defects in fused silica, *The Journal*  
842 *of Chemical Physics*. 64 (1976) 2623–2631. <https://doi.org/10.1063/1.432516>.
- 843 [93] H. Behrens, J. Roux, D.R. Neuville, M. Siemann, Quantification of dissolved H<sub>2</sub>O in silicate glasses  
844 using confocal microRaman spectroscopy, *Chemical Geology*. 229 (2006) 96–112.  
845 <https://doi.org/10.1016/j.chemgeo.2006.01.014>.
- 846 [94] T. Beuvier, M. Richard-Plouet, L. Brohan, Accurate Methods for Quantifying the Relative Ratio of  
847 Anatase and TiO<sub>2</sub> (B) Nanoparticles, *J. Phys. Chem. C*. 113 (2009) 13703–13706.  
848 <https://doi.org/10.1021/jp903755p>.
- 849 [95] I.I. Kornilov, V.V. Vavilova, L.E. Fykin, R.P. Ozerov, S.P. Solowiev, V.P. Smirnov, Neutron  
850 diffraction investigation of ordered structures in the titanium-oxygen system, *Metallurgical*  
851 *Transactions*. 1 (1970) 2569. <https://doi.org/10.1007/BF03038386>.
- 852 [96] I. Farnan, P.J. Grandinetti, J.H. Baltisberger, J.F. Stebbins, U. Werner, M.A. Eastman, A. Pines,  
853 Quantification of the disorder in network-modified silicate glasses, *Nature*. 358 (1992) 31–35.  
854 <https://doi.org/10.1038/358031a0>.
- 855 [97] S. Wang, J.F. Stebbins, Multiple-Quantum Magic-Angle Spinning 17O NMR Studies of Borate,  
856 Borosilicate, and Boroaluminate Glasses, *Journal of the American Ceramic Society*. 82 (1999)  
857 1519–1528. <https://doi.org/10.1111/j.1151-2916.1999.tb01950.x>.
- 858 [98] F. Angeli, T. Charpentier, S. Gin, J.C. Petit, 17O 3Q-MAS NMR characterization of a sodium  
859 aluminoborosilicate glass and its alteration gel, *Chemical Physics Letters*. 341 (2001) 23–28.  
860 [https://doi.org/10.1016/S0009-2614\(01\)00423-7](https://doi.org/10.1016/S0009-2614(01)00423-7).
- 861 [99] F. Angeli, T. Charpentier, M. Gaillard, P. Jollivet, Influence of zirconium on the structure of pristine  
862 and leached soda-lime borosilicate glasses: Towards a quantitative approach by 17O MQMAS  
863 NMR, *Journal of Non-Crystalline Solids*. 354 (2008) 3713–3722.  
864 <https://doi.org/10.1016/j.jnoncrysol.2008.03.046>.
- 865 [100] K.J.D. MacKenzie, M.E. Smith, eds., *Multinuclear solid-state NMR of inorganic materials*,  
866 Pergamon, Amsterdam, 2002.
- 867 [101] S.K. Lee, J.F. Stebbins, Nature of Cation Mixing and Ordering in Na-Ca Silicate Glasses and Melts,  
868 *J. Phys. Chem. B*. 107 (2003) 3141–3148. <https://doi.org/10.1021/jp027489y>.
- 869 [102] T.M. Clark, P.J. Grandinetti, P. Florian, J.F. Stebbins, Correlated structural distributions in silica  
870 glass, *Phys. Rev. B*. 70 (2004) 064202. <https://doi.org/10.1103/PhysRevB.70.064202>.
- 871 [103] N.M. Trease, T.M. Clark, P.J. Grandinetti, J.F. Stebbins, S. Sen, Bond length-bond angle correlation  
872 in densified silica—Results from 17O NMR spectroscopy, *J. Chem. Phys.* 146 (2017) 184505.  
873 <https://doi.org/10.1063/1.4983041>.
- 874 [104] E. Scolan, C. Magenet, D. Massiot, C. Sanchez, Surface and bulk characterisation of titanium–oxo  
875 clusters and nanosized titania particles through 17O solid state NMR, *J. Mater. Chem.* 9 (1999)  
876 2467–2474. <https://doi.org/10.1039/A903714D>.
- 877 [105] R.D. Shannon, Revised effective ionic radii and systematic studies of interatomic distances in  
878 halides and chalcogenides, *Acta Crystallographica Section A*. 32 (1976) 751–767.  
879 <https://doi.org/10.1107/S0567739476001551>.
- 880 [106] X. Cong, R.J. Kirkpatrick, 17O MAS NMR Investigation of the Structure of Calcium Silicate  
881 Hydrate Gel, *Journal of the American Ceramic Society*. 79 (1996) 1585–1592.  
882 <https://doi.org/10.1111/j.1151-2916.1996.tb08768.x>.

- 883 [107] X. Cong, R.J. Kirkpatrick,  $^{29}\text{Si}$  and  $^{17}\text{O}$  NMR investigation of the structure of some crystalline  
884 calcium silicate hydrates, *Advanced Cement Based Materials*. 3 (1996) 133–143.  
885 [https://doi.org/10.1016/S1065-7355\(96\)90045-0](https://doi.org/10.1016/S1065-7355(96)90045-0).
- 886 [108] M.F. Best, R.A. Condrate, A raman study of  $\text{TiO}_2\text{-SiO}_2$  glasses prepared by sol-gel processes, *J*  
887 *Mater Sci Lett*. 4 (1985) 994–998. <https://doi.org/10.1007/BF00721102>.
- 888 [109] K.L. Walther, A. Wokaun, B.E. Handy, A. Baiker,  $\text{TiO}_2/\text{SiO}_2$  mixed oxide catalysts prepared by  
889 sol–gel techniques. Characterization by solid state CP/MAS spectroscopy, *Journal of Non-*  
890 *Crystalline Solids*. 134 (1991) 47–57. [https://doi.org/10.1016/0022-3093\(91\)90010-4](https://doi.org/10.1016/0022-3093(91)90010-4).
- 891 [110] J.P. Rainho, J. Rocha, L.D. Carlos, R.M. Almeida,  $^{29}\text{Si}$  nuclear-magnetic-resonance and vibrational  
892 spectroscopy studies of  $\text{SiO}_2\text{-TiO}_2$  powders prepared by the sol-gel process, *J. Mater. Res*. 16  
893 (2001) 2369–2376. <https://doi.org/10.1557/JMR.2001.0325>.
- 894 [111] M.J. Davis, P.D. Ihinger, A.C. Lasaga, Influence of water on nucleation kinetics in silicate melt,  
895 *Journal of Non-Crystalline Solids*. 219 (1997) 62–69. [https://doi.org/10.1016/S0022-  
896 \*3093\(97\)00252-4\*.](https://doi.org/10.1016/S0022-3093(97)00252-4)
- 897 [112] J. Deubener, R. Müller, H. Behrens, G. Heide, Water and the glass transition temperature of silicate  
898 melts, *Journal of Non-Crystalline Solids*. 330 (2003) 268–273. [https://doi.org/10.1016/S0022-  
899 \*3093\(03\)00472-1\*.](https://doi.org/10.1016/S0022-3093(03)00472-1)
- 900 [113] P. Del Gaudio, H. Behrens, J. Deubener, Viscosity and glass transition temperature of hydrous float  
901 glass, *Journal of Non-Crystalline Solids*. 353 (2007) 223–236.  
902 <https://doi.org/10.1016/j.jnoncrysol.2006.11.009>.
- 903 [114] E.D. Zanotto, The formation of unusual glasses by sol-gel processing, *Journal of Non-Crystalline*  
904 *Solids*. 147–148 (1992) 820–823. [https://doi.org/10.1016/S0022-3093\(05\)80723-9](https://doi.org/10.1016/S0022-3093(05)80723-9).
- 905 [115] E.D. Zanotto, J.C. Mauro, The glassy state of matter: Its definition and ultimate fate, *Journal of Non-*  
906 *Crystalline Solids*. 471 (2017) 490–495. <https://doi.org/10.1016/j.jnoncrysol.2017.05.019>.
- 907 [116] J.F. White, J. Lee, O. Hessling, B. Glaser, Reactions Between Liquid  $\text{CaO-SiO}_2$  Slags and Graphite  
908 Substrates, *Metallurgical and Materials Transactions B*. 48 (2017) 506–515.  
909 <https://doi.org/10.1007/s11663-016-0788-5>.
- 910 [117] V.O. Sokolov, V.G. Plotnichenko, E.M. Dianov, Quantum-chemical modeling of titanium centers  
911 in titanosilicate glass, *Inorganic Materials*. 42 (2006) 1273–1288.  
912 <https://doi.org/10.1134/S0020168506110173>.
- 913 [118] G.A. Tompsett, G.A. Bowmaker, R.P. Cooney, J.B. Metson, K.A. Rodgers, J.M. Seakins, The  
914 Raman spectrum of brookite,  $\text{TiO}_2$  (Pbca,  $Z = 8$ ), *J. Raman Spectrosc*. 26 (1995) 57–62.  
915 <https://doi.org/10.1002/jrs.1250260110>.
- 916 [119] H.L. Ma, J.Y. Yang, Y. Dai, Y.B. Zhang, B. Lu, G.H. Ma, Raman study of phase transformation of  
917  $\text{TiO}_2$  rutile single crystal irradiated by infrared femtosecond laser, *Applied Surface Science*. (2007)  
918 4.
- 919 [120] G. Urbain, Y. Bottinga, P. Richet, Viscosity of liquid silica, silicates and alumino-silicates,  
920 *Geochimica et Cosmochimica Acta*. 46 (1982) 1061–1072. [https://doi.org/10.1016/0016-  
921 \*7037\(82\)90059-X\*.](https://doi.org/10.1016/0016-7037(82)90059-X)
- 922

## 923 **Research data**

924 Research Data associated with this article can be accessed on the repository “[www.zenodo.org](http://www.zenodo.org)” using the  
925 following link: <https://doi.org/10.5281/zenodo.6513443> .